

Aligning Few-Step Diffusion Models with Dense Reward Difference Learning

Ziyi Zhang, Li Shen, Sen Zhang, Deheng Ye, Yong Luo*, Miaojing Shi, Dongjing Shan*,
Bo Du*, *Senior Member, IEEE*, and Dacheng Tao, *Fellow, IEEE*

Abstract—Few-step diffusion models enable efficient high-resolution image synthesis but struggle to align with specific downstream objectives due to limitations of existing reinforcement learning (RL) methods in low-step regimes with limited state spaces and suboptimal sample quality. To address this, we propose Stepwise Diffusion Policy Optimization (SDPO), a novel RL framework tailored for few-step diffusion models. SDPO introduces a dual-state trajectory sampling mechanism, tracking both noisy and predicted clean states at each step to provide dense reward feedback and enable low-variance, mixed-step optimization. For further efficiency, we develop a latent similarity-based dense reward prediction strategy to minimize costly dense reward queries. Leveraging these dense rewards, SDPO optimizes a dense reward difference learning objective that enables more frequent and granular policy updates. Additional refinements, including stepwise advantage estimates, temporal importance weighting, and step-shuffled gradient updates, further enhance long-term dependency, low-step priority, and gradient stability. Our experiments demonstrate that SDPO consistently delivers superior reward-aligned results across diverse few-step settings and tasks. Code is available at <https://github.com/ZiyiZhang27/sdpo>.

Index Terms—Diffusion models, text-to-image, few-step diffusion, reinforcement learning, dense rewards.

I. INTRODUCTION

RECENT studies [1], [4]–[14] have demonstrated progress in distilling standard text-to-image diffusion models [15]–[18] into *few-step* generators, significantly reducing the number of denoising steps needed for high-resolution image synthesis. However, these few-step diffusion models may not inherently align with specific downstream objectives, such

as aesthetic quality [19] or user preferences [3], [20]–[22], which are typically evaluated through reward-based metrics.

Reinforcement learning (RL) finetuning [2], [23], [24] offers a promising approach for aligning diffusion models with reward-driven objectives. However, most existing RL methods are primarily designed for standard diffusion models, where state trajectories are sampled with a uniform number of steps (e.g., 20-50 steps). When naively applied to the *few-step* regime (e.g., 1-4 steps), these methods falter in training stability due to the limited state space and suboptimal sample quality of few-step trajectories, leading to insufficient signal diversity for effective reward optimization. On the other hand, incorporating extended trajectories (e.g., 8-50 steps) can enhance output quality and state coverage, but it also leads to overfitting to *sparse, final-step* rewards that lack dense guidance for intermediate *low-step* predictions, ultimately impairing few-step performance. While mixed-step optimization broadens step coverage by leveraging sample-reward pairs from trajectories of varying lengths, the resulting high variance across such heterogeneous trajectories destabilizes policy optimization.

To address these challenges, we first introduce a *dual-state trajectory sampling* mechanism that leverages the strong single-step denoising capability of advanced few-step diffusion models to concurrently track both the *noisy state* and the *predicted clean state* (an intermediate estimate of the final image) at each step. By mapping final outputs from trajectories of varying lengths onto a shared sequence of intermediate clean states, this mechanism enables *dense, stepwise* reward feedback over uniform-step trajectories, facilitating mixed-step optimization with low variance and consistent denoising dynamics across all steps. This not only mitigates overfitting to the final-step outputs but also avoids the high variance inherent in naive mixed-step optimization. To further improve efficiency, we propose a *dense reward prediction* strategy based on *latent similarity*. Instead of querying rewards at every step, we query only at adaptively selected anchor steps and infer the rest via similarity-weighted interpolation, grounded in a smoothness assumption based on Lipschitz continuity.

Leveraging these dense rewards, we formulate a *dense reward difference learning* objective that optimizes stepwise reward differences rather than aggregated trajectory returns, enabling more frequent and granular policy updates compared to trajectory-level methods [25], [26]. Building on this, we propose *Stepwise Diffusion Policy Optimization* (SDPO), a novel RL finetuning framework tailored for few-step diffusion

Ziyi Zhang, Yong Luo, and Bo Du are with the School of Computer Science, National Engineering Research Center for Multimedia Software and Hubei Key Laboratory of Multimedia and Network Communication Engineering, Wuhan University, Wuhan 430072, China (e-mail: ziyizhang27@whu.edu.cn; yluo180@gmail.com; dubo@whu.edu.cn).

Li Shen is with the School of Cyber Science and Technology, Shenzhen Campus of Sun Yat-sen University, Shenzhen 518107, China (e-mail: mathshenli@gmail.com).

Sen Zhang is with TikTok, ByteDance, Sydney, NSW 2000, Australia (e-mail: senzhang.thu10@gmail.com).

Deheng Ye is with Tencent Inc., Shenzhen 518052, China (e-mail: deri-cye@tencent.com).

Miaojing Shi is with the College of Electronic and Information Engineering, Tongji University, Shanghai 201804, China (e-mail: mshi@tongji.edu.cn).

Dongjing Shan is with the School of Medical Information and Engineering, Southwest Medical University, Luzhou 646000, Sichuan, China (e-mail: shandongjing@swmu.edu.cn).

Dacheng Tao is with the College of Computing and Data Science and the Generative AI Lab at Nanyang Technological University, 50 Nanyang Avenue, Singapore 639798 (e-mail: dacheng.tao@gmail.com).

*Corresponding authors: Yong Luo; Dongjing Shan; Bo Du.

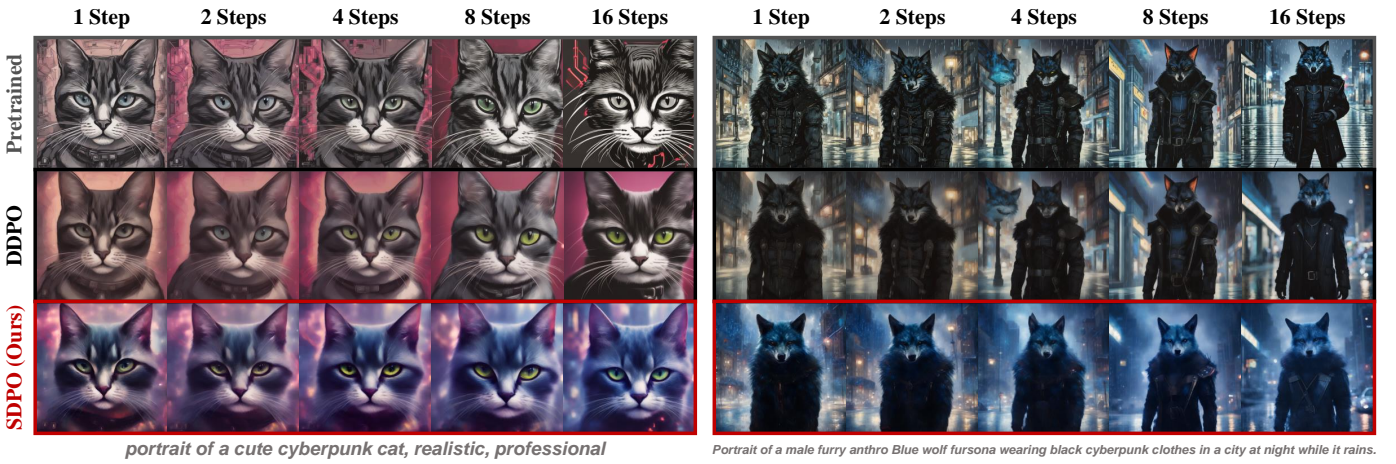


Fig. 1. **Generated images for unseen prompts from:** a pretrained few-step diffusion model (SD-Turbo [1]), and models finetuned with DDPO [2] and our SDPO, both using PickScore [3] and the same number of training samples. All images are generated using the same random seed (42). Our SDPO consistently delivers high-quality, reward-aligned images across various few-step settings, whereas DDPO falters in generating high-quality few-step samples and yields noticeably blurrier images than even the pretrained model.

models. SDPO integrates dual-state sampling to derive dense rewards and incorporates long-term temporal dependencies by computing stepwise advantage estimates, thereby establishing a more robust *stepwise reward difference learning objective*. Additionally, SDPO prioritizes critical low-step optimization through a *temporal importance weighting* strategy and further enhances training stability with *step-shuffled gradient updates*. Together, these innovations empower SDPO to achieve robust and efficient reward optimization, especially in extremely low-step regimes where existing methods tend to falter.

Experimental results show that SDPO excels in reward optimization under extremely low-step regimes, across diverse tasks such as text-to-image generation and multiview image synthesis. Our main contributions are summarized as follows:

- We introduce a dual-state trajectory sampling mechanism tailored for few-step diffusion models, enabling dense reward feedback and low-variance mixed-step optimization.
- We develop a latent similarity-based dense reward prediction strategy that minimizes costly reward queries.
- We formulate a dense reward difference learning objective, allowing few-step diffusion models to effectively optimize dense reward differences at individual steps.
- We propose the unified SDPO framework, which further enhances dense reward difference learning by stepwise advantage difference learning, temporal importance weighting, and step-shuffled updates for more robust and efficient optimization in extremely low-step regimes.

II. PRELIMINARIES

A. Diffusion Models

Denosing diffusion probabilistic models [27] generate high-quality samples by iteratively transforming noise into complex data distributions through a denoising process. In text-to-image applications, these models typically condition each denoising step on a text prompt \mathbf{c} and are operated in two key phases: a forward process that gradually adds noise to an initial sample \mathbf{x}_0 at each step $t \in \{1, \dots, T-1\}$, resulting in progressively

noisier samples \mathbf{x}_t ; and a reverse process that iteratively estimates the conditional distribution $p_\theta(\mathbf{x}_{t-1}|\mathbf{x}_t, \mathbf{c})$ at each step to remove noise and reconstruct the original data.

During the reverse process, each denoising step t yields an estimate of the underlying clean sample \mathbf{x}_0 , often referred to as the *predicted original sample* or *denoised sample*, denoted as $\hat{\mathbf{x}}_0^{t-1}$. For instance, in DDIM [28], each denoising step t starts by estimating the noise component $\epsilon_\theta(\mathbf{x}_t, t, \mathbf{c})$ from the input sample \mathbf{x}_t . This estimated noise is then used to compute the next predicted original sample $\hat{\mathbf{x}}_0^{t-1}$ as:

$$\hat{\mathbf{x}}_0^{t-1} = (\mathbf{x}_t - \sqrt{1 - \bar{\alpha}_t} \cdot \epsilon_\theta(\mathbf{x}_t, t, \mathbf{c})) / \sqrt{\bar{\alpha}_t}, \quad (1)$$

where $\bar{\alpha}_t$ is the cumulative product of the noise scaling factors α_t up to step t . This intermediate prediction of the clean image is progressively refined at each subsequent step.

B. Reinforcement Learning Finetuning for Diffusion Models

Denosing as a Markov decision process (MDP). To perform RL finetuning for diffusion models, existing works [2], [24] formulate the denoising process of diffusion models as a T -step MDP, which is defined as follows:

$$s_t \triangleq (\mathbf{c}, \mathbf{x}_{T-t}), \quad a_t \triangleq \mathbf{x}_{T-t-1}, \quad (2)$$

$$\pi(a_t|s_t) \triangleq p_\theta(\mathbf{x}_{T-t-1}|\mathbf{x}_{T-t}, \mathbf{c}), \quad (3)$$

$$r(s_t, a_t) \triangleq \begin{cases} R(\mathbf{x}_0, \mathbf{c}), & \text{if } t = T - 1 \\ 0, & \text{otherwise,} \end{cases} \quad (4)$$

where the denoising process p_θ governed by diffusion model parameters θ serves as the policy. Starting from an initial noisy state \mathbf{x}_T , at each step t , the policy treats the denoised sample \mathbf{x}_{T-t} as the current state s_t , and the next state \mathbf{x}_{T-t-1} as the action a_t . Rewards are defined sparsely, with only the final state \mathbf{x}_0 being evaluated via the reward function R . The RL objective is thus to maximize the expected reward of final denoising outputs conditioned on prompts $\mathbf{c} \sim p(\mathbf{c})$, i.e.,

$$\min_{\theta} \mathbb{E}_{p(\mathbf{c})} \mathbb{E}_{p_\theta(\mathbf{x}_0|\mathbf{c})} [-R(\mathbf{x}_0, \mathbf{c})]. \quad (5)$$

Optimization via policy gradient. Framing the denoising process as a diffusion policy enables exact computation of log-likelihoods and their gradients w.r.t. the diffusion model parameters θ . Given a full denoising trajectory $\mathbf{x}_{0:T}$, we can specifically compute the log-likelihood $\log p_\theta(\mathbf{x}_{t-1}|\mathbf{x}_t, \mathbf{c})$ for each denoising step. This allows for the computation of the log-likelihood gradient $\nabla_\theta \log p_\theta(\mathbf{x}_{t-1}|\mathbf{x}_t, \mathbf{c})$, which captures the sensitivity of each transition probability to changes in the model parameters. By exploiting this property, existing works [2], [24] apply policy gradient methods [29], [30] to estimate the gradients of Eq. (5) as follows:

$$\mathbb{E}_{p(\mathbf{c})}\mathbb{E}_{p_\theta(\mathbf{x}_{0:T}|\mathbf{c})} \left[-R(\mathbf{x}_0, \mathbf{c}) \sum_{t=1}^T \nabla_\theta \log p_\theta(\mathbf{x}_{t-1}|\mathbf{x}_t, \mathbf{c}) \right]. \quad (6)$$

Reward difference learning. Inspired by direct preference optimization (DPO) [31] that converts the RL objective for language models into a supervised classification objective, recent approaches [25], [26] further derive a mean squared error-based objective for diffusion models, where the goal is to match the differences in log-likelihood ratios with the differences in rewards across paired denoising trajectories:

$$\mathbb{E}_{\mathbf{x}^a, \mathbf{x}^b, \mathbf{c}} \left[\sum_{t=1}^T \left(\frac{1}{\eta} \left(\log \frac{p_\theta(\mathbf{x}_t^a|\mathbf{c})}{p_{\theta'}(\mathbf{x}_t^a|\mathbf{c})} - \log \frac{p_\theta(\mathbf{x}_t^b|\mathbf{c})}{p_{\theta'}(\mathbf{x}_t^b|\mathbf{c})} \right) - (R(\mathbf{x}_0^a, \mathbf{c}) - R(\mathbf{x}_0^b, \mathbf{c})) \right)^2 \right]. \quad (7)$$

Here, \mathbf{x}_t^a and \mathbf{x}_t^b represent paired samples from the denoising step t of two independent trajectories, both generated using the same text prompt \mathbf{c} . These paired samples are used to compute the differences in their corresponding rewards, i.e., $R(\mathbf{x}_0^a, \mathbf{c}) - R(\mathbf{x}_0^b, \mathbf{c})$, as well as the differences in their log-likelihood ratios. In particular, $\log \frac{p_\theta(\mathbf{x}_t^a|\mathbf{c})}{p_{\theta'}(\mathbf{x}_t^a|\mathbf{c})}$ denotes the log-likelihood ratio of the sample \mathbf{x}_t^a under the current model parameters θ compared to the previous or reference model parameters θ' , helping to quantify the change in the model during online optimization. Furthermore, the *log-ratio scale factor* η balances the contribution of log-ratio differences relative to reward differences in the objective. Empirically, both Deng et al. [25] and Gao et al. [26] demonstrate that this reward difference-based approach results in more stable reward optimization for diffusion models, compared to vanilla policy gradient methods [2], [24].

III. METHOD

A. Limitations of Existing RL Finetuning for Few-Step Diffusion Models

Existing RL finetuning methods for diffusion models typically rely on a fixed, uniform number of denoising steps per trajectory (e.g., 50 steps). While effective for standard diffusion models, this uniform-step paradigm introduces critical challenges in RL Finetuning for few-step diffusion models. In the target few-step regime (e.g., 1 to 4 steps), short sampling trajectories result in limited state spaces and inherently suboptimal output quality, yielding insufficient signal diversity for

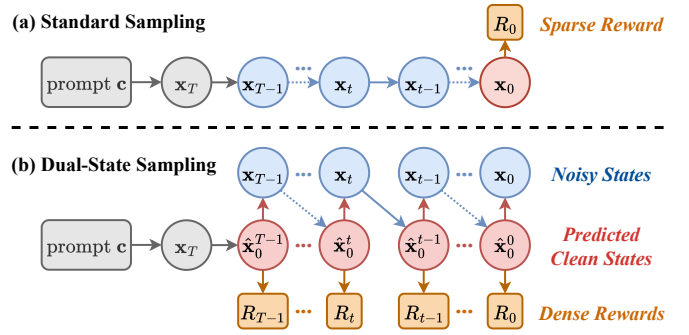


Fig. 2. **Dual-state sampling vs. standard sampling.** Unlike the standard sampling process of diffusion models, our dual-state sampling approach maps final outputs from trajectories of varying lengths onto a shared sequence of intermediate clean states $\{\hat{\mathbf{x}}_0^t\}_{t=0}^{T-1}$, enabling dense reward feedback over a mixed-step trajectory with low variance and consistent denoising dynamics.

reliable policy updates. As a result, naively applying uniform-step RL finetuning to few-step diffusion models leads to unstable training dynamics and poor sample efficiency (as evidenced by the reward curves in Fig. 7).

On the other hand, using extended trajectories (e.g., 8 to 50 steps) can generate higher-quality samples and expand the state space. However, this approach has its own drawbacks. Without dense, step-by-step reward feedback for intermediate low-step samples, the model tends to overfit to the longer trajectories, undermining its few-step inference ability (see the reward curves for low-step samples in Fig. 4). However, deriving dense rewards for intermediate steps is not straightforward, since most existing reward functions are designed to evaluate final clean images rather than the noisy intermediate states typical of denoising processes. One potential solution is to mix trajectories of different lengths, providing rewards at various sampling steps. While this can offer more generalization, the inconsistent dynamics across trajectories introduce significant variance, which destabilizes policy optimization and undermines training consistency (as evidenced by the reward curves in the right plot of Fig. 7).

B. Mixed-Step Trajectories with Consistent Dynamics

To address these challenges, we propose a *dual-state sampling* mechanism that enables dense, stepwise reward feedback over uniform-step trajectories, facilitating mixed-step trajectory optimization with low variance and consistent denoising dynamics across all steps. Crucially, while naive mixed-step denoising trajectories suffer from high variance due to inconsistent denoising dynamics, this dual-state sampling mechanism maps final outputs from trajectories of varying lengths onto a *shared, consistent* sequence of predicted clean states $\{\hat{\mathbf{x}}_0^t\}_{t=0}^{T-1}$ across all steps, effectively reducing this variance.

Dual-state sampling. As discussed in Section II-A, the *predicted original sample* $\hat{\mathbf{x}}_0^{t-1}$ serves as an intermediate estimate of the *final, noise-free* data at the corresponding denoising step t . Due to the strong single-step denoising capacity distilled into few-step diffusion models, this intermediate estimate remains highly accurate even during early denoising steps, allowing $\hat{\mathbf{x}}_0^{t-1}$ to act as a reliable *surrogate* for the

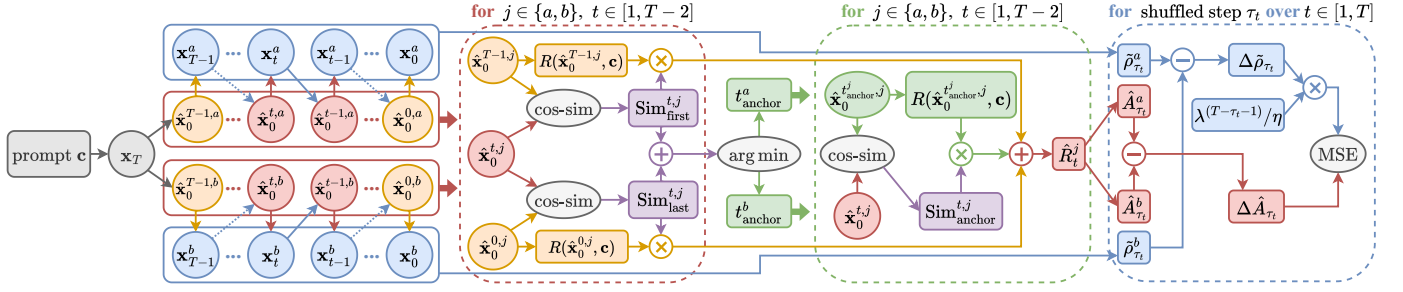


Fig. 3. **SDPO framework.** SDPO first samples a pair of *dual-state trajectories* $\{\mathbf{x}_t^a, \hat{\mathbf{x}}_0^{t,a}\}_{t=0}^{T-1}$ and $\{\mathbf{x}_t^b, \hat{\mathbf{x}}_0^{t,b}\}_{t=0}^{T-1}$ using a shared *prompt* c and *initial noise* \mathbf{x}_T . It then queries the *reward function* R for clean states at the *first*, *final*, and *anchor* (t_{anchor}) steps and predicts *dense rewards* \hat{R}_t for other steps via latent similarity, ultimately yielding the *stepwise advantage estimate* \hat{A}_t . Finally, at each *shuffled step* τ_t , the MSE loss between the *advantage difference* $\Delta \hat{A}_{\tau_t}$ and the *log-ratio difference* $\Delta \hat{\rho}_{\tau_t}$ (weighted by $\lambda^{(T-\tau_t-1)}/\eta$) is computed.

final output of a full t -step denoising process. Building on this insight, our dual-state sampling mechanism concurrently tracks two states throughout the trajectory: the *noisy state* \mathbf{x}_{t-1} and the predicted *clean state* $\hat{\mathbf{x}}_0^{t-1}$. As illustrated in Fig. 2 (b), at each sampling step t , we first denoise the previous noisy state \mathbf{x}_t to compute the predicted clean state $\hat{\mathbf{x}}_0^{t-1}$ via Eq. (1). The next noisy state \mathbf{x}_{t-1} is then derived by combining $\hat{\mathbf{x}}_0^{t-1}$ with the directional noise component:

$$\mathbf{x}_{t-1} = \sqrt{\bar{\alpha}_{t-1}} \hat{\mathbf{x}}_0^{t-1} + \sqrt{1 - \bar{\alpha}_{t-1}} \cdot \epsilon_{\theta}(\mathbf{x}_t, t, c). \quad (8)$$

This approach preserves the trajectory's stochastic dynamics while maintaining a direct link to intermediate clean estimates, laying the foundation for the dense reward feedback.

Dense reward feedback via $\hat{\mathbf{x}}_0^t$. The dual-state sampling mechanism enables us to evaluate and assign dense, step-level rewards at each intermediate denoising step t by leveraging the predicted clean estimates $\hat{\mathbf{x}}_0^{t-1}$ within the dual-state trajectory, rather than relying solely on sparse rewards from the final-step outputs. Accordingly, we redefine the trajectory reward in the denoising MDP (Eq. (4)) by applying the predefined reward function R to each intermediate clean state $\hat{\mathbf{x}}_0^{T-t-1}$:

$$r(s_t, a_t) \triangleq R(\hat{\mathbf{x}}_0^{T-t-1}, c). \quad (9)$$

This reformulation ensures that each denoising step contributes directly to policy optimization, guided by the quality of its corresponding clean estimate. By decoupling trajectory length from reward structure, our approach not only prevents overfitting to the high-step, final outputs of uniform-length trajectories, but also eliminates the high variance inherent in naive mixed-step trajectories. This yields a more balanced mixed-step optimization paradigm, where the progressive refinement of $\hat{\mathbf{x}}_0^t$ over steps drives consistent and stable optimization.

C. Dense Reward Difference Learning for Few-Step Diffusion Models

Although our dual-state sampling enables dense rewards from intermediate clean states, directly decoding the latent-space states to image space for reward queries remains computationally prohibitive. To address this, we propose an efficient dense reward prediction strategy based on latent similarity, reducing reward queries while maintaining robust and granular guidance throughout the denoising process.

Dense reward prediction via latent similarity. Rather than querying rewards at every denoising step, we limit reward queries to three per trajectory: two fixed queries at the first and last steps, and one query at an adaptively selected intermediate step, referred to as the *anchor step* (t_{anchor}). To determine the anchor step, we first calculate the cosine similarity between the latent representations of each predicted clean state $\hat{\mathbf{x}}_0^t$ and those at the first and last steps, respectively:

$$\text{Sim}_{\text{first}}^t = \frac{\langle \hat{\mathbf{x}}_0^t, \hat{\mathbf{x}}_0^{T-1} \rangle}{\|\hat{\mathbf{x}}_0^t\| \|\hat{\mathbf{x}}_0^{T-1}\|}, \quad \text{Sim}_{\text{last}}^t = \frac{\langle \hat{\mathbf{x}}_0^t, \hat{\mathbf{x}}_0^0 \rangle}{\|\hat{\mathbf{x}}_0^t\| \|\hat{\mathbf{x}}_0^0\|}. \quad (10)$$

The anchor step is then identified as the step that minimizes the sum of cosine similarities to the first and last steps:

$$t_{\text{anchor}} = \arg \min_{t \in \{1, \dots, T-2\}} (\text{Sim}_{\text{first}}^t + \text{Sim}_{\text{last}}^t), \quad (11)$$

which effectively selects the step that is most distinct from both endpoints in the latent space. This adaptive selection strategy is grounded in information theory and optimal sampling principles [32], [33], aiming to maximize the total information gained from the limited reward queries by minimizing redundancy among them. By choosing an anchor step that is minimally correlated with two extremes of the trajectory, we ensure that the three queried steps provide maximal insight into the dense reward landscape, thereby enhancing the reliability of subsequent reward predictions for unqueried steps.

With rewards queried at these three steps, we predict the dense reward \hat{R}_t for each intermediate step t by performing a similarity-weighted interpolation of the queried rewards:

$$\hat{R}_t = \frac{R_{T-1} \cdot \text{Sim}_{\text{first}}^t + R_{t_{\text{anchor}}} \cdot \text{Sim}_{\text{anchor}}^t + R_0 \cdot \text{Sim}_{\text{last}}^t}{\text{Sim}_{\text{first}}^t + \text{Sim}_{\text{anchor}}^t + \text{Sim}_{\text{last}}^t} \quad (12)$$

where R_{T-1} , $R_{t_{\text{anchor}}}$, and R_0 denote the rewards queried at the first, anchor, and last steps, respectively, and $\text{Sim}_{\text{anchor}}^t$ is the cosine similarity between $\hat{\mathbf{x}}_0^t$ and $\hat{\mathbf{x}}_0^{t_{\text{anchor}}}$. This interpolation leverages the latent similarities to effectively estimate rewards for unqueried steps, providing dense feedback while minimizing the number of costly reward function evaluations.

Smoothness assumption via Lipschitz continuity. Our dense reward prediction strategy is grounded in a smoothness assumption: the composition of the reward function R with the latent encoder ϕ satisfies a Lipschitz condition. Formally, there exists a constant $K_R > 0$ such that

$$|R(\hat{\mathbf{x}}_0^i, c) - R(\hat{\mathbf{x}}_0^j, c)| \leq K_R \|\phi(\hat{\mathbf{x}}_0^i) - \phi(\hat{\mathbf{x}}_0^j)\|. \quad (13)$$

This Lipschitz property ensures that small perturbations in the latent representation lead to bounded changes in reward values, justifying our use of latent similarity as a reliable proxy for reward interpolation. This assumption holds for many practical reward functions, particularly those based on perceptual quality or semantic alignment, which typically exhibit smooth variations with respect to image content.

Dense reward difference learning. Leveraging dense rewards derived from two independent dual-state trajectories, i.e., \hat{R}_t^a and \hat{R}_t^b , we formulate a dense reward difference learning objective that aligns the difference in *dense rewards* with the difference in *log-likelihood ratios* at each step t . Specifically, we define the log-likelihood ratio for each trajectory as $\rho_t^j(\theta) := \log(p_\theta(\mathbf{x}_t^j|\mathbf{c})/p_{\theta'}(\mathbf{x}_t^j|\mathbf{c}))$, where $j \in \{a, b\}$. The objective is then formulated as:

$$\mathbb{E}_{\mathbf{x}_t^a, \mathbf{x}_t^b, \mathbf{c}} \left[\left(\frac{1}{\eta} (\rho_t^a(\theta) - \rho_t^b(\theta)) - (\hat{R}_t^a - \hat{R}_t^b) \right)^2 \right], \quad (14)$$

where θ' refers to the previous model parameters. By eliminating the need to accumulate full trajectory data, this stepwise objective enables more frequent and granular updates compared to trajectory-level objectives like Eq. (7).

D. Stepwise Diffusion Policy Optimization

Building on the dual-state sampling mechanism from Section III-B and the dense reward difference learning objective from Section III-C, we propose *Stepwise Diffusion Policy Optimization* (SDPO), a novel RL finetuning framework designed to effectively optimize few-step diffusion models through stepwise, dense reward feedback. Unlike existing methods that optimize final outputs from full trajectories monolithically, SDPO exploits the stepwise granularity of intermediate clean states and their dense rewards to tackle the unique challenges inherent in optimizing few-step denoising outputs, while ensuring stable and efficient policy updates.

Dual-state trajectory integration. First, SDPO unifies dual-state trajectory sampling from Section III-B and dense reward difference learning from Section III-C within a single Markovian framework. Leveraging the dual-state sampling mechanism, SDPO simultaneously tracks the noisy state \mathbf{x}_t (for policy rollouts) and its corresponding predicted clean state $\hat{\mathbf{x}}_0^t$ (for dense reward prediction via Eq. (12)) at each step t . Incorporated with the dense reward difference learning objective, SDPO generates two independent dual-state trajectories $\{\mathbf{x}_t^a, \hat{\mathbf{x}}_0^{t,a}\}_{t=0}^{T-1}$ and $\{\mathbf{x}_t^b, \hat{\mathbf{x}}_0^{t,b}\}_{t=0}^{T-1}$ under the same initial noise \mathbf{x}_T and prompt $\mathbf{c} \sim p(\mathbf{c})$. In contrast to standard reward difference learning methods that use independently initialized noise for each trajectory, SDPO shares initial noise between each trajectory pair to reduce variance in log-likelihoods, thereby leading to more stable and efficient policy updates.

Stepwise advantage difference learning. While Eq. (14) enables granular, step-by-step policy updates, it overlooks the temporal dependencies inherent in the denoising process, where early denoising steps shape later outcomes. To address this, SDPO incorporates long-term feedback from future steps into the current step's evaluation by computing a *discounted return* \hat{G}_t^j for each trajectory $j \in \{a, b\}$ at step t , aggregating

Algorithm 1 Stepwise Diffusion Policy Optimization

- 1: **Input:** Pretrained diffusion model parameters θ , prompt distribution $p(\mathbf{c})$, number of training epochs E , number of denoising timesteps per trajectory T , batch size B
 - 2: **for** epoch $e = 1, \dots, E$ **do**
 - 3: Sample a batch of text prompts $\{\mathbf{c}_i \sim p(\mathbf{c})\}_{i=1}^B$
 - 4: *Phase 1: Trajectory Sampling (no gradient)*
 - 5: **for** mini-batch $i = 1, \dots, B$ **do**
 - 6: Generate dual-state trajectory $\{\mathbf{x}_t^{a,i}, \hat{\mathbf{x}}_0^{t,a,i}\}_{t=0}^{T-1}$
 - 7: Generate dual-state trajectory $\{\mathbf{x}_t^{b,i}, \hat{\mathbf{x}}_0^{t,b,i}\}_{t=0}^{T-1}$
 - 8: Compute dense rewards $\{\hat{R}_t^{a,i}, \hat{R}_t^{b,i}\}_{t=0}^{T-1}$
 - 9: Compute discounted returns $\{\hat{G}_t^{a,i}, \hat{G}_t^{b,i}\}_{t=0}^{T-1}$
 - 10: Generate shuffled step indices $\{\tau_t^i\}_{t=0}^{T-1}$
 - 11: **end for**
 - 12: Compute advantage estimates $\{\hat{A}_t^{a,i}, \hat{A}_t^{b,i}\}_{t=0}^{T-1}$
 - 13: *Phase 2: Policy Update (with gradient)*
 - 14: **for** timestep $t = 1, \dots, T$ **do**
 - 15: Re-generate next states at shuffled steps $\{\tau_t^i\}_{i=1}^B$
 - 16: Compute log-likelihoods at shuffled steps $\{\tau_t^i\}_{i=1}^B$
 - 17: Update θ by minimizing $\mathcal{L}_t(\theta)$ in Eq.(18)
 - 18: **end for**
 - 19: **end for**
-

dense rewards from future steps with a discount factor $\gamma \in (0, 1]$, i.e., $\hat{G}_t^j = \sum_{k=0}^t \gamma^k \hat{R}_{t-k}^j$. To reduce variance across trajectories while preserving inter-step relationships, SDPO performs a novel *per-step-prompt normalization* mechanism on \hat{G}_t^j , maintaining running estimates of the mean μ_t and standard deviation σ_t for each step-prompt pair. This yields *stepwise advantage estimates* \hat{A}_t^j , which quantify relative improvement over baseline performance. By substituting rewards in Eq. (14) with these stepwise advantage estimates, SDPO induces a *stepwise advantage difference learning* objective:

$$\mathbb{E}_{\mathbf{x}_t^a, \mathbf{x}_t^b, \mathbf{c}} \left[\left(\frac{1}{\eta} (\rho_t^a(\theta) - \rho_t^b(\theta)) - (\hat{A}_t^a - \hat{A}_t^b) \right)^2 \right]. \quad (15)$$

Temporal importance weighting. To prioritize optimization for low-step samples while still utilizing later-step samples for broader state space exploration, we introduce a *temporal importance weighting* strategy in SDPO's dense reward difference learning objective. This is achieved by applying an exponentially decaying weight, controlled by the *decay rate* λ , to the log-likelihood ratios. Specifically, the weight for a sample at step t is defined as $\lambda^{(T-t-1)}$, decreasing from the first step ($t = T - 1$) to the last step ($t = 0$). In practice, this means that the log-ratio difference, $\Delta\rho_t(\theta) := \rho_t^a(\theta) - \rho_t^b(\theta)$, is scaled by $\lambda^{(T-t-1)}/\eta$ and matched against the corresponding advantage difference, $\Delta\hat{A}_t := \hat{A}_t^a - \hat{A}_t^b$. Thus, the weighted objective function for each step t can be formulated as:

$$l_\theta = \mathbb{E}_{\mathbf{x}_t^a, \mathbf{x}_t^b, \mathbf{c}} \left[\left(\Delta\rho_t(\theta) \cdot \lambda^{(T-t-1)}/\eta - \Delta\hat{A}_t \right)^2 \right]. \quad (16)$$

Additionally, to prevent large, unstable policy updates, we clip the log-likelihood ratios at a threshold ϵ , defining $\tilde{\rho}_t^j(\theta) := \text{clip}(\rho_t^j(\theta), -\epsilon, \epsilon)$, yielding the clipped objective:

$$\tilde{l}_\theta = \mathbb{E}_{\mathbf{x}_t^a, \mathbf{x}_t^b, \mathbf{c}} \left[\left(\Delta\tilde{\rho}_t(\theta) \cdot \lambda^{(T-t-1)}/\eta - \Delta\hat{A}_t \right)^2 \right]. \quad (17)$$

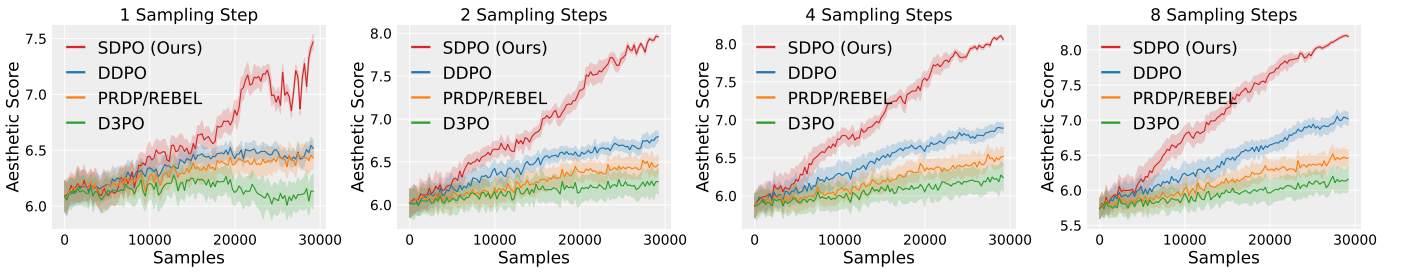


Fig. 4. **Reward curves for low-step samples**, where reward scores are evaluated and averaged over 1-, 2-, 4-, and 8-step samples. The horizontal axis shows the cumulative number of training samples, equivalent to the number of training iterations multiplied by the batch size, which is consistent across all methods.

Step-shuffled gradient updates. Leveraging the stepwise granularity of our advantage estimates, SDPO performs gradient updates individually for each step rather than aggregating over entire trajectories. However, sequential stepwise updates risk overfitting to the fixed step order of trajectories. To address this, we introduce step-shuffled gradient updates, where the step order within each mini-batch of trajectories is independently shuffled. As illustrated in Algorithm 1, SDPO conducts T gradient updates per training epoch, with T being the number of steps per trajectory. For the t -th update, gradient estimates are computed by averaging over B mini-batches of stepwise samples $(\mathbf{x}_{\tau_t^i}^{a,i}, \mathbf{x}_{\tau_t^i}^{b,i}, \mathbf{c}_i)$, where τ_t^i denotes the shuffled step index for the i -th mini-batch. Accordingly, the empirical training objective of SDPO is defined as:

$$\mathcal{L}_t(\theta) \leftarrow \frac{1}{B} \sum_{i=1}^B \max \left(l_\theta(\mathbf{x}_{\tau_t^i}^{a,i}, \mathbf{x}_{\tau_t^i}^{b,i}, \mathbf{c}_i), \tilde{l}_\theta(\mathbf{x}_{\tau_t^i}^{a,i}, \mathbf{x}_{\tau_t^i}^{b,i}, \mathbf{c}_i) \right), \quad (18)$$

where the maximization between the objectives l_θ and \tilde{l}_θ serves to minimize an upper bound on the policy updates. The overall framework of SDPO is illustrated in Fig. 3.

IV. EXPERIMENTS

A. Main Experimental Setup

In our main experiments (Sections IV-B and IV-C), we use SD-Turbo [1], a few-step text-to-image model distilled from Stable Diffusion v2.1 [16] through adversarial diffusion distillation [1], as the base model. For efficient finetuning, we apply Low-Rank Adaptation (LoRA) [34], which enables updating only the LoRA weights while freezing the pretrained model parameters. Following DDPO [2], we generate denoising trajectories during training using the DDIM sampler [28] and a prompt set of 45 animal names. Since SD-Turbo does not support classifier-free guidance or negative prompts, we disable them by setting the guidance scale to 1.0. We implement four commonly used reward functions: Aesthetic Score [19], ImageReward [20], HPSv2 [21], and PickScore [3].

B. Algorithm Comparisons

We compare our SDPO against established reward finetuning methods for diffusion models, selecting representatives from three distinct categories. For policy gradient methods, we adopt DDPO [2] due to its proven effectiveness in this domain. For reward difference-based approaches, we initially

targeted PRDP [25], but its lack of open-source availability led us to implement REBEL [26] instead; however, encountering mode collapse with REBEL on SD-Turbo prompted us to introduce clipping from PRDP, resulting in an interpolated 'PRDP/REBEL' method that mitigates this issue. For preference-based methods, such as Diffusion-DPO [36] and KTO [37], we note that they typically prioritize learning from data-driven preferences rather than explicit reward functions, distinguishing their objectives from ours. Nevertheless, we adopt D3PO [35], another state-of-the-art DPO-style method for diffusion models, which leverages preference relationships from relative rewards, enabling reward-based finetuning aligned with our settings. To ensure a fair comparison, we standardize all shared hyperparameters across algorithms (implementation details are presented in the appendix).

Sample efficiency in optimizing low-step samples. Sample efficiency measures how effectively algorithms leverage samples to enhance reward outcomes. We evaluate this by generating samples from intermediate model checkpoints using various step configurations and assessing their reward scores. Fig. 4 displays Aesthetic Score reward curves for images generated with 1, 2, 4, and 8 sampling steps, while additional reward curves are provided in the appendix. In these plots, the x-axis specifies the cumulative number of samples used for training, and the y-axis indicates the average reward of low-step samples. The steeper reward curves of SDPO suggest that it is able to achieve higher rewards with fewer samples compared to other algorithms, demonstrating its superior sample efficiency in optimizing low-step samples.

Generalization to unseen prompts. We further evaluate the generalization capability of our SDPO on unseen, complex text prompts from [24], specifying attributes like color (*A green colored rabbit*), count (*Four wolves in the park*), composition (*A cat and a dog*), and location (*A dog on the moon*). Accordingly, Table I presents reward scores for 1-, 2-, 4-, and 8-step samples generated from these unseen prompts by both the non-finetuned SD-Turbo and various finetuned models. Notably, SDPO consistently outperforms all baselines across different reward functions and step settings. Qualitative results on unseen prompts are provided in Fig. 1 and the appendix.

C. Ablation Study

In this subsection, we conduct a series of ablation studies on SDPO's core components, providing comprehensive experimental analysis to validate their individual contributions to

TABLE I

GENERALIZATION TO UNSEEN PROMPTS. WE REPORT REWARD SCORES FOR 1-, 2-, 4-, AND 8-STEP SAMPLES GENERATED FROM UNSEEN PROMPTS BY BOTH THE NON-FINETUNED BASE MODEL (LABELED AS SD-TURBO) AND THE FINETUNED MODELS OF DIFFERENT RL FINETUNING METHODS.

Method	ImageReward				Aesthetic Score				HPSv2				PickScore			
	1s	2s	4s	8s	1s	2s	4s	8s	1s	2s	4s	8s	1s	2s	4s	8s
SD-Turbo [1]	1.126	1.101	1.038	0.976	6.064	5.955	5.842	5.745	27.85	28.22	28.41	28.26	22.69	22.88	22.91	22.68
D3PO [35]	1.292	1.211	1.176	1.210	6.292	6.208	6.159	6.116	28.06	28.51	28.77	28.78	22.64	22.95	23.16	23.00
DDPO [2]	1.380	1.252	1.378	1.387	6.644	6.584	6.595	6.720	28.54	28.75	28.99	29.05	22.65	22.94	23.04	23.29
REBEL [26]	1.280	1.305	1.289	1.294	6.509	6.471	6.472	6.418	28.28	28.58	28.87	28.97	22.61	22.86	23.01	23.19
SDPO (Ours)	1.719	1.559	1.545	1.601	7.062	7.516	7.867	8.163	28.77	29.14	29.35	29.36	23.02	23.22	23.60	24.05

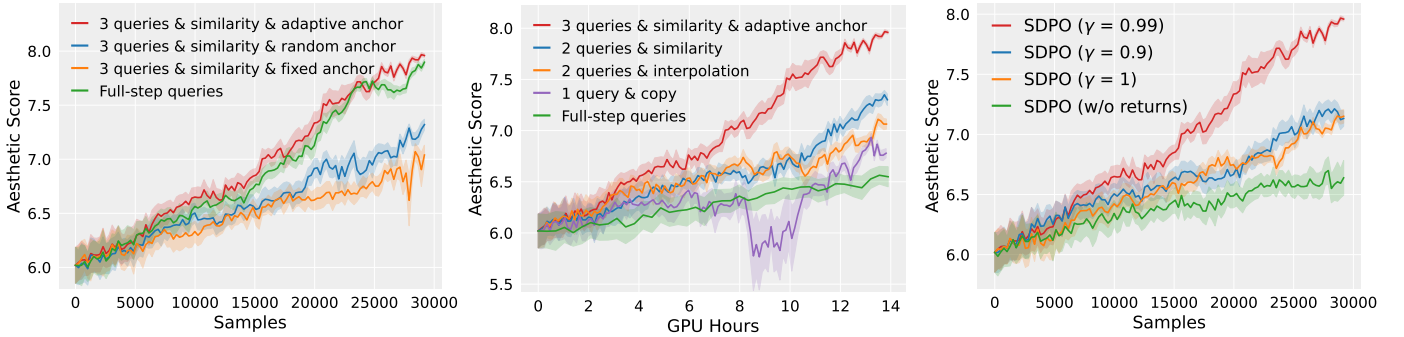


Fig. 5. Ablation study on dense reward prediction (left & middle) and discounted returns (right) for SDPO.

overall reward optimization performance, particularly in two-step denoising outputs. While reward functions like PickScore, HPSv2, and ImageReward benefit from explicit text-image alignment supervision, our ablation studies focus on the Aesthetic Score reward, which lacks such guidance and thus makes the reward optimization task more challenging.

Effect of dense reward prediction. As detailed in Section III-C, we use 3 reward queries per trajectory, latent similarity, and an adaptively selected anchor to efficiently predict dense rewards. To examine the effectiveness of this approach, we compare SDPO with variants that employ alternative strategies for dense reward prediction, including:

- *3 queries & similarity & adaptive anchor*: Original setup.
- *3 queries & similarity & random anchor*: In this variant, we retain the 3 reward queries per trajectory and the latent similarity computation, but select the anchor randomly instead of via adaptive criteria.
- *3 queries & similarity & fixed anchor*: In this setup, we again use 3 reward queries and latent similarity but set a fixed anchor at the 25th step for all trajectories.
- *2 queries & similarity*: Here, we reduce the number of reward queries from 3 to 2, retaining the latent similarity computation while eliminating the anchor selection.
- *2 queries & interpolation*: In this method, we also use 2 reward queries but replace the latent similarity method with simple interpolation to approximate dense rewards.
- *1 query & copy*: Here, we restrict reward queries to the final step, copying it to all intermediate steps and avoiding dense reward prediction—a common strategy used by most existing methods such as DDPO and REBEL.
- *Full-step queries*: This variant involves querying the reward function at every step of the trajectory, maximizing the reward density without any interpolation.

The left plot in Fig. 5 compares the sample efficiency of these variants by plotting the reward scores of two-step denoising outputs against training samples, while the middle plot further compares time efficiency by plotting reward scores against GPU hours. Notably, our original setup (*3 queries & similarity & adaptive anchor*) consistently outperforms all variants in terms of both sample and time efficiency, underscoring the reliability and effectiveness of our dense reward prediction strategy. Interestingly, the *full-step queries* variant, despite its maximal reward-query density, actually underperforms our method. This is likely due to the additional noise and variance introduced by direct per-step reward querying, which can destabilize policy updates. In contrast, our interpolation-based approach provides implicit regularization that smooths out such fluctuations while retaining essential reward dynamics, thereby facilitating more stable and efficient optimization. Moreover, the superior time efficiency of our method further highlights its practical advantages in delivering reliable dense rewards with minimal computational overhead.

Effect of discounted returns. We then evaluate SDPO with different discount factors: $\gamma = 0.99$, 0.9 , and 1 , along with a variant that directly uses rewards without returns. As shown in the right plot of Fig. 5, SDPO with $\gamma = 0.99$ achieves the best performance in sample efficiency.

Effect of per-step-prompt normalization. We also compare the per-step-prompt normalization strategy in SDPO with two alternatives: (1) *per-prompt normalization*, which normalizes rewards on a per-prompt basis, and (2) *global normalization*, which simply normalizes rewards across all samples. The left plot in Fig. 6 shows both alternatives underperform our per-step-prompt normalization. However, the per-prompt normalization variant still outperforms baseline methods, which also use per-prompt normalization, indicating

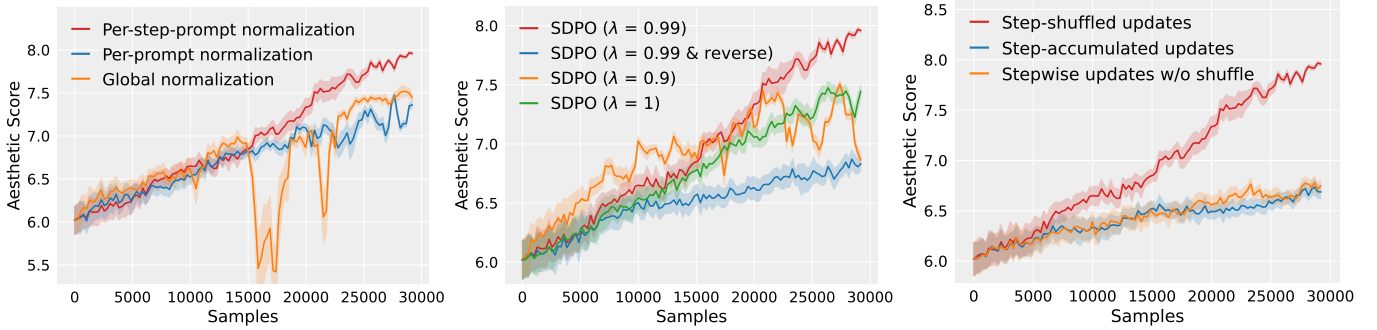


Fig. 6. Ablation study on return normalization (left), importance weighting (middle), and gradient updates (right) for SDPO.

TABLE II
COMPARISON OF SIMILARITY BETWEEN PREDICTED AND DIRECTLY QUERIED REWARDS ACROSS DIFFERENT METHODS.

Reward Function	Method	Cosine Similarity \uparrow	L1 Distance \downarrow	L2 Distance \downarrow
Aesthetic Score	1 query & copy	2×10^{-8}	11630	131
	2 queries & interpolation	0.3368	11228	130
	2 queries & similarity	0.3861	9771	125
	3 queries & similarity & fixed anchor	0.3654	9832	127
	3 queries & similarity & random anchor	0.3561	9744	128
	3 queries & similarity & adaptive anchor (Ours)	0.4463	9073	119
ImageReward	1 query & copy	2×10^{-8}	11262	130
	2 queries & interpolation	0.3901	10561	125
	2 queries & similarity	0.4078	9340	123
	3 queries & similarity & fixed anchor	0.3611	9423	128
	3 queries & similarity & random anchor	0.3924	9337	125
	3 queries & similarity & adaptive anchor (Ours)	0.4683	8598	117
HPSv2	1 query & copy	3×10^{-8}	11411	129
	2 queries & interpolation	0.3696	10798	127
	2 queries & similarity	0.3676	9915	127
	3 queries & similarity & fixed anchor	0.3253	9886	131
	3 queries & similarity & random anchor	0.3648	9955	128
	3 queries & similarity & adaptive anchor (Ours)	0.4549	9009	118
PickScore	1 query & copy	3×10^{-8}	11540	131
	2 queries & interpolation	0.4307	10237	121
	2 queries & similarity	0.4117	9318	123
	3 queries & similarity & fixed anchor	0.3933	9368	125
	3 queries & similarity & random anchor	0.3846	9324	126
	3 queries & similarity & adaptive anchor (Ours)	0.4853	8657	115

that our dense reward strategy is reliable on its own.

Effect of temporal importance weighting. We further analyze the impact of temporal importance weighting in SDPO with different decay factors: $\lambda = 0.99$, 0.9 , and 1 , as well as a variant that applies weights in a *reverse* order. The middle plot in Fig. 6 shows that SDPO with $\lambda = 0.99$ yields the best performance, while removing weighting ($\lambda = 1$) or applying reverse weighting degrades performance. Nonetheless, the variant with no weighting still outperforms baseline methods, further confirming the reliability of our dense reward strategy.

Effect of step-shuffled gradient updates. Finally, we evaluate the impact of replacing step-shuffled updates in SDPO with two alternatives: (1) *step-accumulated updates* and (2) *stepwise updates without shuffling*. As shown in the right plot in Fig. 6, step-accumulated updates, which accumulate gradients across all denoising steps before a single model update, reduce sample efficiency compared to our step-shuffled updates. Additionally, stepwise updates performed sequentially without shuffling the step order also exhibit reduced sample

efficiency, due to overfitting to the fixed step order.

D. Analysis of Dense Reward Prediction Accuracy

To further substantiate the effectiveness of our dense reward prediction strategy, we compare dense rewards predicted by different strategies (from the ablation study in Section IV-C) against ground-truth rewards directly queried from target reward functions along full trajectories. Specifically, we evaluate the similarity between predicted and queried rewards using cosine similarity as well as L1 and L2 distances. To address scale differences among reward functions, all rewards are normalized to the range $[0, 1]$ before computing these metrics. As summarized in Table II, our method consistently achieves the highest cosine similarity and lowest L1/L2 distances across all evaluated reward functions compared to alternative strategies. This demonstrates the effectiveness of our dense reward prediction strategy in capturing representative and reliable reward dynamics with limited reward queries.

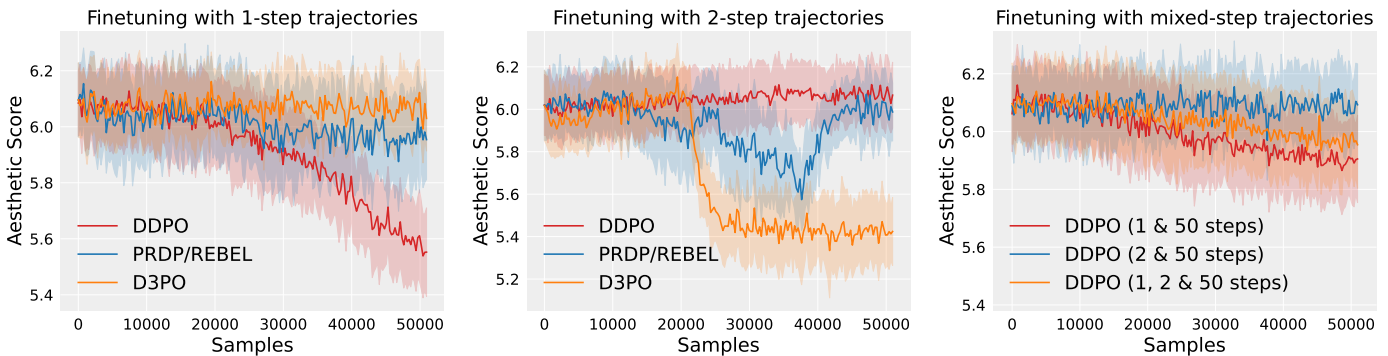


Fig. 7. **Analysis of the instability of existing methods in finetuning with few-step or mixed-step trajectories.** We present the reward optimization curves of DDPO, PRDP/REBEL, and D3PO during finetuning SD-Turbo with **1-step** (left) and **2-step** (middle) denoising trajectories, as well as the reward optimization of DDPO during finetuning with **mixed-step** trajectories (right).

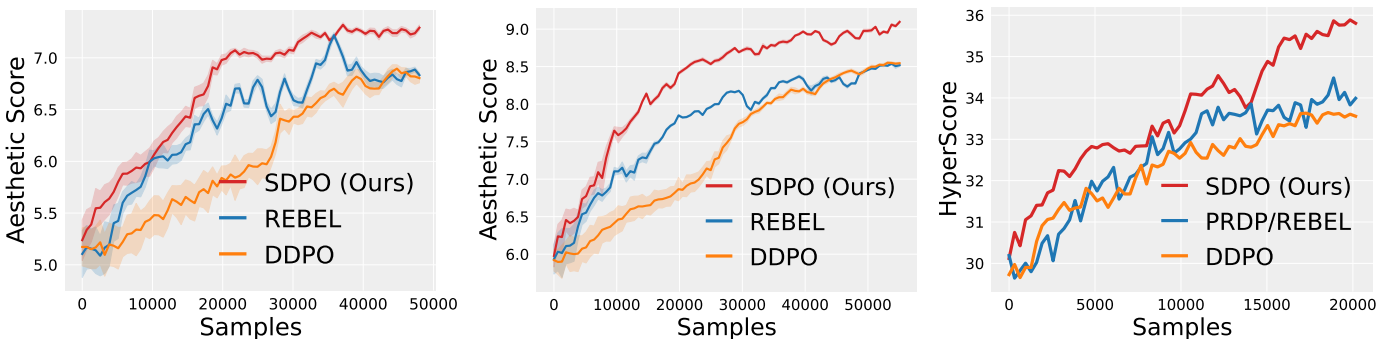


Fig. 8. **Reward curves for latent consistency model** (left: 1-step sampling; middle: 8-step sampling) and **text-to-multiview diffusion model** (right).

E. Instability of Existing Methods in Finetuning with Few-Step and Mixed-Step Trajectories

As discussed in Section III-A, we evaluate the training instability of existing methods (DDPO, PRDP/REBEL, and D3PO) when finetuning SD-Turbo with extremely few-step trajectories (e.g., 1 or 2 steps). The left and middle plots of Fig. 7 illustrate the reward optimization curves of these methods during finetuning with 1-step and 2-step denoising trajectories, respectively. The results reveal significant instability in reward optimization across all methods, characterized by large fluctuations and occasional collapses in reward scores over training iterations. This instability arises from the diminished quality and diversity of low-step samples, which lack sufficient information for the policy to distinguish subtle behaviors or assess long-term outcomes accurately.

Moreover, the right plot of Fig. 7 further displays the reward optimization curves of DDPO when finetuning with mixed-step trajectories. Here, we observe that DDPO still suffers from similar instability, as the mixed-step trajectories introduce additional variance and complexity into the training process. These findings underscore the challenges faced by existing methods in effectively leveraging few-step and mixed-step trajectories for stable and efficient reward optimization. In contrast to these methods, which rely on individual trajectories of varying lengths, our SDPO employs dual-state sampling within uniform-length trajectories to generate intermediate clean states that emulate outputs from varying-length trajectories. By incorporating this design with dense reward feedback,

SDPO leverages consistent and informative training signals, thereby facilitating a balanced, stable optimization process.

F. Extension to Latent Consistency Models

We further conduct extensive experiments on finetuning consistency models with our SDPO. To achieve this, we utilize the RLCM framework [38], which applies both DDPO and REBEL for finetuning a latent consistency model (LCM) [8] distilled from Dreamshaper v7 [39]. As shown in Fig. 8, SDPO achieves superior sample efficiency over DDPO and REBEL in finetuning the LCM on Aesthetic Score, even when evaluated under the most challenging 1-step sampling setting, further validating its effectiveness in extremely low-step regimes.

G. Extension to Text-to-Multiview Diffusion Models

We also evaluate SDPO on the multiview image generation task. Specifically, we employ LCM-SDXL [40] with the MV-Adapter [41] as the base model and the HyperScore metric from the MATE-3D benchmark [42] as the reward function. As illustrated in Fig. 8 (right), SDPO consistently outperforms competing methods in finetuning the text-to-multiview diffusion model on HyperScore.

V. RELATED WORK

Diffusion model alignment. Existing approaches for diffusion alignment [43]–[45] can be broadly classified into two categories: (1) reward-based methods, which use techniques such as policy gradient [2], [24], [46]–[51], reward

difference [25], [26], or reward backpropagation through sampling [52]–[55] to optimize the model based on explicit reward functions; and (2) preference-based methods [35]–[37], [56]–[60], which employ DPO-style objectives to directly align the model with data-driven preferences. Our work falls into the first category, focusing on aligning few-step diffusion models.

Reward finetuning of few-step diffusion models. Recent approaches [61], [62] incorporate reward guidance into consistency distillation, while not directly applicable to other distilled few-step models. RLCM [38] introduces an RL finetuning framework specifically for consistency models, which we use as a baseline in our extensive analysis of consistency models. In contrast, we extend RL finetuning to a wider range of few-step diffusion models and address the challenge of optimizing extremely low-step samples.

Dense feedback for diffusion models. Recent studies have explored dense feedback in diffusion alignment. For RL finetuning, Zhang et al. [46] highlight the importance of dense rewards to prevent overoptimization, and introduce a temporal critic to estimate dense rewards. For preference learning, Yang et al. [56] apply temporal discounting in a DPO-style objective to distinguish preferences at each step, while Liang et al. [58] build a step-aware preference model to provide stepwise preference. In contrast, our work incorporates dense rewards into RL finetuning of few-step diffusion models without requiring additional model training.

VI. CONCLUSION

This paper presents SDPO, a novel framework for RL finetuning of few-step diffusion models. By unifying dual-state trajectory sampling with dense reward feedback in a stepwise advantage difference learning paradigm, SDPO enables stable and efficient reward optimization, especially in extremely low-step regimes where existing methods falter. Future work may explore extending SDPO to a wider range of reward functions and state-of-the-art models, as well as integrating it with advanced RL finetuning techniques such as Flow-GRPO [51], to further evaluate and enhance its performance and scalability across diverse diffusion model alignment scenarios.

ACKNOWLEDGMENTS

This work was supported in part by the National Natural Science Foundation of China under Grant 62225113, Grant U23A20318, and Grant 62276195, in part by the Science and Technology Major Project of Hubei Province under Grant 2025BCB026 and Grant 2024BAB046, in part by the Foundation for Innovative Research Groups of Hubei Province under Grant 2024AFA017. The work of Li Shen was supported in part by NSFC under Grant 62576364, in part by Shenzhen Basic Research Project (Natural Science Foundation) Basic Research Key Project under Grant JCYJ20241202124430041, in part by CCF-Tencent Rhino-Bird Open Research Fund under Grant CCF-Tencent RAGR20250114 and Grant Tencent JR2025TEG002. Dr Tao’s research is partially supported by NTU RSR and Start Up Grants. This work was also supported by WHU-Kingsoft Joint Lab. The numerical calculations in this paper have been done on the supercomputing system in the Supercomputing Center of Wuhan University.

REFERENCES

- [1] A. Sauer, D. Lorenz, A. Blattmann, and R. Rombach, “Adversarial diffusion distillation,” in *European Conference on Computer Vision*, 2024, pp. 87–103.
- [2] K. Black, M. Janner, Y. Du, I. Kostrikov, and S. Levine, “Training diffusion models with reinforcement learning,” in *International Conference on Learning Representations*, 2024.
- [3] Y. Kirstain, A. Polyak, U. Singer, S. Matiana, J. Penna, and O. Levy, “Pick-a-pic: An open dataset of user preferences for text-to-image generation,” *Advances in Neural Information Processing Systems*, vol. 36, pp. 36 652–36 663, 2023.
- [4] T. Salimans and J. Ho, “Progressive distillation for fast sampling of diffusion models,” in *International Conference on Learning Representations*, 2022.
- [5] C. Meng, R. Rombach, R. Gao, D. Kingma, S. Ermon, J. Ho, and T. Salimans, “On distillation of guided diffusion models,” in *Proceedings of the IEEE/CVF Conference on Computer Vision and Pattern Recognition*, 2023, pp. 14 297–14 306.
- [6] W. Luo, T. Hu, S. Zhang, J. Sun, Z. Li, and Z. Zhang, “Diff-Instruct: A universal approach for transferring knowledge from pre-trained diffusion models,” *Advances in Neural Information Processing Systems*, vol. 36, pp. 76 525–76 546, 2023.
- [7] Y. Song, P. Dhariwal, M. Chen, and I. Sutskever, “Consistency models,” in *International Conference on Machine Learning*, 2023, pp. 32 211–32 252.
- [8] S. Luo, Y. Tan, L. Huang, J. Li, and H. Zhao, “Latent Consistency Models: Synthesizing high-resolution images with few-step inference,” *arXiv preprint arXiv:2310.04378*, 2023.
- [9] D. Kim, C.-H. Lai, W.-H. Liao, N. Murata, Y. Takida, T. Uesaka, Y. He, Y. Mitsufuji, and S. Ermon, “Consistency trajectory models: Learning probability flow ODE trajectory of diffusion,” in *The Twelfth International Conference on Learning Representations*, 2024.
- [10] X. Liu, X. Zhang, J. Ma, J. Peng, and Q. Liu, “Instafflow: One step is enough for high-quality diffusion-based text-to-image generation,” in *International Conference on Learning Representations*, 2024.
- [11] S. Lin, A. Wang, and X. Yang, “SDXL-Lightning: Progressive adversarial diffusion distillation,” *arXiv preprint arXiv:2402.13929*, 2024.
- [12] T. Yin, M. Gharbi, R. Zhang, E. Shechtman, F. Durand, W. T. Freeman, and T. Park, “One-step diffusion with distribution matching distillation,” in *Proceedings of the IEEE/CVF Conference on Computer Vision and Pattern Recognition*, 2024, pp. 6613–6623.
- [13] T. Yin, M. Gharbi, T. Park, R. Zhang, E. Shechtman, F. Durand, and W. T. Freeman, “Improved distribution matching distillation for fast image synthesis,” *Advances in Neural Information Processing Systems*, vol. 37, 2024.
- [14] T. H. Nguyen and A. Tran, “SwiftBrush: One-step text-to-image diffusion model with variational score distillation,” in *Proceedings of the IEEE/CVF Conference on Computer Vision and Pattern Recognition*, 2024, pp. 7807–7816.
- [15] J. Sohl-Dickstein, E. Weiss, N. Maheswaranathan, and S. Ganguli, “Deep unsupervised learning using nonequilibrium thermodynamics,” in *International Conference on Machine Learning*, 2015, pp. 2256–2265.
- [16] R. Rombach, A. Blattmann, D. Lorenz, P. Esser, and B. Ommer, “High-resolution image synthesis with latent diffusion models,” in *Proceedings of the IEEE/CVF Conference on Computer Vision and Pattern Recognition*, 2022, pp. 10 684–10 695.
- [17] D. Podell, Z. English, K. Lacey, A. Blattmann, T. Dockhorn, J. Müller, J. Penna, and R. Rombach, “SDXL: Improving latent diffusion models for high-resolution image synthesis,” in *International Conference on Learning Representations*, 2024.
- [18] P. Esser, S. Kulal, A. Blattmann, R. Entezari, J. Müller, H. Saini, Y. Levi, D. Lorenz, A. Sauer, F. Boesel, D. Podell, T. Dockhorn, Z. English, and R. Rombach, “Scaling rectified flow transformers for high-resolution image synthesis,” in *International Conference on Machine Learning*, 2024, pp. 12 606–12 633.
- [19] C. Schuhmann, R. Beaumont, R. Vencu, C. W. Gordon, R. Wightman, M. Cherti, T. Coombes, A. Katta, C. Mullis, M. Wortsman, P. Schramowski, S. R. Kundurthy, K. Crowson, L. Schmidt, R. Kaczmarczyk, and J. Jitsev, “LAION-5B: An open large-scale dataset for training next generation image-text models,” *Advances in Neural Information Processing Systems*, vol. 35, pp. 25 278–25 294, 2022.
- [20] J. Xu, X. Liu, Y. Wu, Y. Tong, Q. Li, M. Ding, J. Tang, and Y. Dong, “ImageReward: Learning and evaluating human preferences for text-to-image generation,” *Advances in Neural Information Processing Systems*, vol. 36, pp. 15 903–15 935, 2023.

- [21] X. Wu, Y. Hao, K. Sun, Y. Chen, F. Zhu, R. Zhao, and H. Li, "Human Preference Score v2: A solid benchmark for evaluating human preferences of text-to-image synthesis," *arXiv preprint arXiv:2306.09341*, 2023.
- [22] Y. Liang, J. He, G. Li, P. Li, A. Klimovskiy, N. Carolan, J. Sun, J. Pont-Tuset, S. Young, F. Yang, J. Ke, K. D. Dvijotham, K. M. Collins, Y. Luo, Y. Li, K. J. Kohlhoff, D. Ramachandran, and V. Navalpakkam, "Rich human feedback for text-to-image generation," in *Proceedings of the IEEE/CVF Conference on Computer Vision and Pattern Recognition*, 2024, pp. 19 401–19 411.
- [23] Y. Fan and K. Lee, "Optimizing DDPM sampling with shortcut fine-tuning," in *International Conference on Machine Learning*, 2023, pp. 9623–9639.
- [24] Y. Fan, O. Watkins, Y. Du, H. Liu, M. Ryu, C. Boutilier, P. Abbeel, M. Ghavamzadeh, K. Lee, and K. Lee, "DPOK: Reinforcement learning for fine-tuning text-to-image diffusion models," *Advances in Neural Information Processing Systems*, vol. 36, pp. 79 858–79 885, 2023.
- [25] F. Deng, Q. Wang, W. Wei, T. Hou, and M. Grundmann, "PRDP: Proximal reward difference prediction for large-scale reward finetuning of diffusion models," in *Proceedings of the IEEE/CVF Conference on Computer Vision and Pattern Recognition*, 2024, pp. 7423–7433.
- [26] Z. Gao, J. D. Chang, W. Zhan, O. Oertell, G. Swamy, K. Brantley, T. Joachims, J. A. Bagnell, J. D. Lee, and W. Sun, "Rebel: Reinforcement learning via regressing relative rewards," *Advances in Neural Information Processing Systems*, vol. 37, pp. 52 354–52 400, 2024.
- [27] J. Ho, A. Jain, and P. Abbeel, "Denoising diffusion probabilistic models," *Advances in Neural Information Processing Systems*, vol. 33, pp. 6840–6851, 2020.
- [28] J. Song, C. Meng, and S. Ermon, "Denoising diffusion implicit models," in *International Conference on Learning Representations*, 2021.
- [29] R. J. Williams, "Simple statistical gradient-following algorithms for connectionist reinforcement learning," *Machine learning*, vol. 8, pp. 229–256, 1992.
- [30] J. Schulman, F. Wolski, P. Dhariwal, A. Radford, and O. Klimov, "Proximal policy optimization algorithms," *arXiv preprint arXiv:1707.06347*, 2017.
- [31] R. Rafailov, A. Sharma, E. Mitchell, C. D. Manning, S. Ermon, and C. Finn, "Direct preference optimization: Your language model is secretly a reward model," *Advances in Neural Information Processing Systems*, vol. 36, pp. 53 728–53 741, 2023.
- [32] M. C. Shewry and H. P. Wynn, "Maximum entropy sampling," *Journal of Applied Statistics*, vol. 14, no. 2, pp. 165–170, 1987.
- [33] A. Belhadji, R. Bardenet, and P. Chainais, "Kernel interpolation with continuous volume sampling," in *International Conference on Machine Learning*, 2020, pp. 725–735.
- [34] E. J. Hu, Y. Shen, P. Wallis, Z. Allen-Zhu, Y. Li, S. Wang, L. Wang, and W. Chen, "LoRA: Low-rank adaptation of large language models," in *International Conference on Learning Representations*, 2022.
- [35] K. Yang, J. Tao, J. Lyu, C. Ge, J. Chen, W. Shen, X. Zhu, and X. Li, "Using human feedback to fine-tune diffusion models without any reward model," in *Proceedings of the IEEE/CVF Conference on Computer Vision and Pattern Recognition*, 2024, pp. 8941–8951.
- [36] B. Wallace, M. Dang, R. Rafailov, L. Zhou, A. Lou, S. Purushwalkam, S. Ermon, C. Xiong, S. Joty, and N. Naik, "Diffusion model alignment using direct preference optimization," in *Proceedings of the IEEE/CVF Conference on Computer Vision and Pattern Recognition*, 2024, pp. 8228–8238.
- [37] S. Li, K. Kallidromitis, A. Gokul, Y. Kato, and K. Kozuka, "Aligning diffusion models by optimizing human utility," *Advances in Neural Information Processing Systems*, vol. 37, pp. 24 897–24 925, 2024.
- [38] O. Oertell, J. D. Chang, Y. Zhang, K. Brantley, and W. Sun, "RL for consistency models: Reward guided text-to-image generation with fast inference," *Reinforcement Learning Journal*, vol. 4, pp. 1656–1673, 2024.
- [39] Lykon, "Lykon/dreamshaper-7," HuggingFace, 2023.
- [40] LCM Team, "latent-consistency/lcm-sdxl," HuggingFace, 2023.
- [41] Z. Huang, Y.-C. Guo, H. Wang, R. Yi, L. Ma, Y.-P. Cao, and L. Sheng, "MV-Adapter: Multi-view consistent image generation made easy," in *Proceedings of the IEEE/CVF International Conference on Computer Vision*, 2025, pp. 16 377–16 387.
- [42] Y. Zhang, B. Cui, Q. Yang, Z. Li, and Y. Xu, "Benchmarking and learning multi-dimensional quality evaluator for text-to-3D generation," in *Proceedings of the IEEE/CVF International Conference on Computer Vision*, 2025, pp. 18 563–18 574.
- [43] K. Lee, H. Liu, M. Ryu, O. Watkins, Y. Du, C. Boutilier, P. Abbeel, M. Ghavamzadeh, and S. S. Gu, "Aligning text-to-image models using human feedback," *arXiv preprint arXiv:2302.12192*, 2023.
- [44] X. Wu, K. Sun, F. Zhu, R. Zhao, and H. Li, "Human Preference Score: Better aligning text-to-image models with human preference," in *Proceedings of the IEEE/CVF International Conference on Computer Vision*, 2023, pp. 2096–2105.
- [45] B. Liu, S. Shao, B. Li, L. Bai, Z. Xu, H. Xiong, J. Kwok, S. Helal, and Z. Xie, "Alignment of diffusion models: Fundamentals, challenges, and future," *arXiv preprint arXiv:2409.07253*, 2024.
- [46] Z. Zhang, S. Zhang, Y. Zhan, Y. Luo, Y. Wen, and D. Tao, "Confronting reward overoptimization for diffusion models: A perspective of inductive and primacy biases," in *International Conference on Machine Learning*, 2024, pp. 60 396–60 413.
- [47] Y. Zhang, E. Tzeng, Y. Du, and D. Kislyuk, "Large-scale reinforcement learning for diffusion models," in *European Conference on Computer Vision*, 2024, pp. 1–17.
- [48] M. Uehara, Y. Zhao, K. Black, E. Hajiramezani, G. Scalia, N. L. Diamant, A. M. Tseng, S. Levine, and T. Biancalani, "Feedback efficient online fine-tuning of diffusion models," in *International Conference on Machine Learning*, 2024, pp. 48 892–48 918.
- [49] S. H. Lee, Y. Li, J. Ke, I. Yoo, H. Zhang, J. Yu, Q. Wang, F. Deng, G. Entis, J. He *et al.*, "Parrot: Pareto-optimal multi-reward reinforcement learning framework for text-to-image generation," in *European Conference on Computer Vision*, 2025, pp. 462–478.
- [50] Z. Zhang, S. Zhang, L. Shen, Y. Zhan, Y. Luo, H. Hu, B. Du, Y. Wen, and D. Tao, "Aligning text-to-image diffusion models with constrained reinforcement learning," *IEEE Transactions on Pattern Analysis and Machine Intelligence*, vol. 47, no. 11, pp. 9550–9562, 2025.
- [51] J. Liu, G. Liu, J. Liang, Y. Li, J. Liu, X. Wang, P. Wan, D. Zhang, and W. Ouyang, "Flow-GRPO: Training flow matching models via online RL," *Advances in Neural Information Processing Systems*, vol. 38, 2025.
- [52] K. Clark, P. Vicol, K. Swersky, and D. J. Fleet, "Directly fine-tuning diffusion models on differentiable rewards," in *International Conference on Learning Representations*, 2024.
- [53] M. Prabhudesai, A. Goyal, D. Pathak, and K. Fragkiadaki, "Aligning text-to-image diffusion models with reward backpropagation," *arXiv preprint arXiv:2310.03739*, 2023.
- [54] M. Prabhudesai, R. Mendonca, Z. Qin, K. Fragkiadaki, and D. Pathak, "Video diffusion alignment via reward gradients," *arXiv preprint arXiv:2407.08737*, 2024.
- [55] X. Wu, Y. Hao, M. Zhang, K. Sun, Z. Huang, G. Song, Y. Liu, and H. Li, "Deep reward supervisions for tuning text-to-image diffusion models," in *European Conference on Computer Vision*, 2024, pp. 108–124.
- [56] S. Yang, T. Chen, and M. Zhou, "A dense reward view on aligning text-to-image diffusion with preference," in *International Conference on Machine Learning*, 2024, pp. 55 998–56 032.
- [57] H. Yuan, Z. Chen, K. Ji, and Q. Gu, "Self-play fine-tuning of diffusion models for text-to-image generation," *Advances in Neural Information Processing Systems*, vol. 37, pp. 73 366–73 398, 2024.
- [58] Z. Liang, Y. Yuan, S. Gu, B. Chen, T. Hang, M. Cheng, J. Li, and L. Zheng, "Aesthetic post-training diffusion models from generic preferences with step-by-step preference optimization," in *Proceedings of the IEEE/CVF Conference on Computer Vision and Pattern Recognition*, 2025, pp. 13 199–13 208.
- [59] S. Karthik, H. Coskun, Z. Akata, S. Tulyakov, J. Ren, and A. Kag, "Scalable ranked preference optimization for text-to-image generation," in *Proceedings of the IEEE/CVF International Conference on Computer Vision*, 2025, pp. 18 399–18 410.
- [60] F.-A. Croitoru, V. Hondru, R. T. Ionescu, N. Sebe, and M. Shah, "Curriculum direct preference optimization for diffusion and consistency models," in *Proceedings of the Computer Vision and Pattern Recognition Conference*, 2025, pp. 2824–2834.
- [61] J. Li, W. Feng, W. Chen, and W. Y. Wang, "Reward guided latent consistency distillation," *Transactions on Machine Learning Research*, 2024.
- [62] Y. Ren, X. Xia, Y. Lu, J. Zhang, J. Wu, P. Xie, X. Wang, and X. Xiao, "Hyper-SD: Trajectory segmented consistency model for efficient image synthesis," *Advances in Neural Information Processing Systems*, vol. 37, pp. 117 340–117 362, 2024.



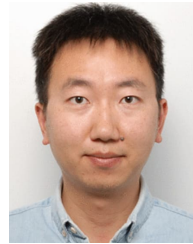
Ziyi Zhang is currently working toward the PhD degree with the School of Computer Science, Wuhan University, China, supervised by Prof. Dr. Yong Luo. His research interests currently focus on generative models (particularly diffusion models) and reinforcement learning from human feedback. He has published several papers in peer-reviewed top-tier journals and conferences, including IEEE TPAMI, ICML, IJCAI, and IEEE TMM. His personal homepage is at <https://ziyizhang27.github.io>.



Yong Luo is currently a Professor with the School of Computer Science, Wuhan University, China. His research interests are primarily on machine learning and data mining with applications to visual information understanding and analysis. He has authored or co-authored over 100 papers in top journals and prestigious conferences including Nature Machine Intelligence, Nature Communications, IEEE T-PAMI and IJCV. He is serving on editorial board for IEEE T-MM and The Innovation Informatics. He received the IEEE Globecom 2016 Best Paper Award, and was nominated as the IJCAI 2017 Distinguished Best Paper Award. He is also a co-recipient of the IEEE TMM 2023, IEEE ICME 2019 and IEEE VCIP 2019 Best Paper Awards.



Li Shen is currently an associate professor at Sun Yat-sen University. Previously, he was a research scientist at JD Explore Academy, Beijing, and a senior researcher at Tencent AI Lab, Shenzhen. He received his bachelor's degree and Ph.D. from the School of Mathematics, South China University of Technology. His research interests include efficient deep learning, efficient reinforcement learning, optimization and deep learning theory. He has served as the senior program committee for AAAI and area chairs for ICML, NeurIPS, ICLR, CVPR, and ACM MM. He is also the associate editor for IEEE Transactions on Pattern Analysis and Machine Intelligence, IEEE Transactions on Knowledge and Data Engineering, and IEEE Transactions on Multimedia.



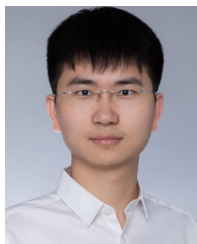
Miaoqing Shi received the Ph.D. degree from Peking University in 2015. He also engaged with a joint PhD program with the University of Oxford and INRIA Rennes for a year. He held a postdoctoral position with the University of Edinburgh and was a research scientist with INRIA Rennes. Between 2020 and 2022, he was a lecturer with the Department of Informatics, King's College London. Since 2023, he has become a full professor with Tongji University and a visiting senior lecturer with King's. He has authored or coauthored more than 50 publications. His current research focus is on visual learning and understanding, with multi-task and limited supervision.



Sen Zhang received the Ph.D. degree from the School of Computer Science at the University of Sydney. He is currently a machine learning engineer at TikTok, ByteDance, Sydney. Previously, he was a postdoctoral research assistant at the University of Sydney. His research interests include computer vision, vSLAM, and foundation models. He has published several papers in top-tier conferences and journals, including IEEE TPAMI, ECCV, IJCV, ICRA, ICML, ICLR, and ACM Multimedia.



Dongjing Shan is currently an Associate Professor with the School of Medical Information and Engineering, Southwest Medical University, Luzhou, Sichuan, China. Previously, he was a Researcher with the Laboratory of Intelligent Information Processing, Army Engineering University, Chongqing, China. He received the B.Eng. degree in computer science from Beijing Institute of Technology, Beijing, China, in 2008, the M.S. degree in information science and technology from Peking University, Beijing, in 2013, and the Ph.D. degree in signal processing from the Speech Processing Laboratory, Army Engineering University, Nanjing, China, in 2020. His research interests include machine learning and deep learning with applications to image processing and speech recognition.



Deheng Ye received the Ph.D. degree from the School of Computer Science and Engineering, Nanyang Technological University, Singapore, in 2016. He is currently the Director of AI Applications at Tencent, Shenzhen, China, where he spearheads a dynamic team of engineers and researchers in the development of large-scale machine learning platforms and intelligent AI agents. His leadership has been instrumental in innovating and integrating pioneering AI technologies into real-world applications, with online AI service requests reaching billions per day worldwide. Apart from industry-level projects, he has authored/co-authored more than 50 academic papers to date. He also regularly serves as PC/SPC for leading venues such as NeurIPS, ICML, ICLR, AAAI, IJCAI, and so on.



Bo Du received the Ph.D. degree in photogrammetry and remote sensing from the State Key Laboratory of Information Engineering in Surveying, Mapping and Remote Sensing, Wuhan University, Wuhan, China, in 2010. He is currently a Professor with the School of Computer Science and the Institute of Artificial Intelligence, Wuhan University. He is also the Director of the National Engineering Research Center for Multimedia and Software, Wuhan University. He has published more than 100 research articles in IEEE Transactions on Pattern Analysis and Machine Intelligence (TPAMI), IEEE Transactions on Image Processing (TIP), IEEE Transactions on Cybernetics (TCYB), IEEE Transactions on Geoscience and Remote Sensing (TGRS), IEEE Journal of Selected Topics in Applied Earth Observations and Remote Sensing (JSTARS), and IEEE Geoscience and Remote Sensing Letters (GRSL). His research interests include pattern recognition, hyperspectral image processing, and signal processing. He received the IEEE Geoscience and Remote Sensing Society (GRSS) 2020 Transactions Prize Paper Award, the IJCAI Distinguished Paper Prize, the IEEE Data Fusion Contest Champion, and the IEEE Workshop on Hyperspectral Image and Signal Processing Best Paper Award in 2018. He has served as the Area Chair for the International Conference on Pattern Recognition (ICPR). He serves as an Associate Editor for Neural Networks, Pattern Recognition, and Neurocomputing.



Dacheng Tao is currently a Distinguished University Professor and the Inaugural Director of the Generative AI Lab in the College of Computing and Data Science at Nanyang Technological University. He was an Australian Laureate Fellow and the founding director of the Sydney AI Centre in the University of Sydney, the inaugural director of JD Explore Academy and senior vice president in JD.com, and the chief AI scientist in UBTECH Robotics. He mainly applies statistics and mathematics to artificial intelligence, and his research is detailed in one

monograph and over 300 publications. His publications have been cited over 140K times and he has an h-index 180+ in Google Scholar. He received the 2015 and 2020 Australian Eureka Prize, the 2018 IEEE ICDM Research Contributions Award, 2020 research super star by The Australian, the 2019 Diploma of The Polish Neural Network Society, and the 2021 IEEE Computer Society McCluskey Technical Achievement Award. He is a Fellow of the Australian Academy of Science, ACM and IEEE.

Aligning Few-Step Diffusion Models with Dense Reward Difference Learning

Supplemental Material

Ziyi Zhang, Li Shen, Sen Zhang, Deheng Ye, Yong Luo*, Miaoqing Shi, Dongjing Shan*,
Bo Du*, *Senior Member, IEEE*, and Dacheng Tao, *Fellow, IEEE*

CONTENTS

Appendix A: Implementation Details	1
A-A Main Experimental Setup	1
A-B Additional Setup for Latent Consistency Models	2
A-C Additional Setup for Text-to-Multiview Diffusion Models	2
Appendix B: Derivations	2
B-A The Gradient of the SDPO Objective	2
Appendix C: Additional Reward Curves	3
Appendix D: Additional Qualitative Examples	5
Appendix E: Validity of Predicted Clean States as Surrogates for Actual t-Step Outputs	9
Appendix F: Empirical Analysis of Lipschitz Continuity Across Reward Functions	9
Appendix G: Comparison of Peak GPU Memory Usage During RL Finetuning	10
Appendix H: Effectiveness of Step-Shuffled Updates in Preventing Step Overfitting	10
Appendix I: Rationale and Advantages of Reward Difference Learning in SDPO	11
Appendix J: Analysis of Complementary Mechanisms for Enhancing Dense Reward Utilization in SDPO	12
Appendix K: Additional Analysis on the Effectiveness of Dense Rewards in SDPO	12
Appendix L: Additional Analysis on Reward Overoptimization via Cross-Reward Generalization Evaluation	13
References	14

APPENDIX A

IMPLEMENTATION DETAILS

A. Main Experimental Setup

We adopt SD-Turbo [1] as the base model for the key experiments described in Sections IV-B and IV-C of the main manuscript. Implementation details for all algorithms, including the baselines, are provided below.

DDPO implementation. We use the official PyTorch codebase of DDPO [2], substituting SD-Turbo as the base model. Since SD-Turbo does not support classifier-free guidance, we disable it by setting the guidance scale to 1.0.

PRDP/REBEL implementation. As PRDP [3] is not open-source, we implement REBEL [4] and incorporate PRDP’s clipping to mitigate mode collapse, forming an interpolated “PRDP/REBEL” method. For a fair comparison, we align shared hyperparameters with DDPO, such as denoising steps, classifier-free guidance scale, learning rate, clipping range, and batch size, except for the log-ratio scale factor, which is set to 1 following [4]. While DDPO generates only one trajectory per batch, PRDP/REBEL produces a pair of trajectories for reward difference learning. To maintain consistent policy rollouts, we halve the number of batches and gradient accumulation steps for PRDP/REBEL. Moreover, to ensure a fair comparison with our SDPO, we also adopt shared initial noise between each trajectory pair in PRDP/REBEL to reduce variance.

D3PO implementation. Finetuning SD-Turbo with D3PO [5] is straightforward, as the official D3PO codebase builds on DDPO. We match shared hyperparameters with DDPO and PRDP/REBEL for fairness, such as denoising steps, classifier-free

guidance scale, learning rate, and batch size. Like PRDP/REBEL, D3PO generates trajectory pairs for preference learning. Thus, we keep the number of batches and gradient accumulation steps per epoch consistent between them.

SDPO implementation. Our SDPO configuration inherits most shared hyperparameters from PRDP/REBEL. By leveraging dense rewards, SDPO eliminates the need to accumulate full trajectories, thus enabling more frequent model updates. To stabilize training under this increased update frequency, we reduce the learning rate of SDPO. Table I lists the key hyperparameters we adopt during finetuning SD-Turbo [1] with SDPO.

Training prompts. We present below the training prompt set of 45 animal names employed in the experiments detailed in Section IV of our main manuscript:

cat	dog	horse	monkey	rabbit	zebra	spider	bird	sheep	deer
cow	goat	lion	tiger	bear	raccoon	fox	wolf	lizard	beetle
ant	butterfly	fish	shark	whale	dolphin	squirrel	mouse	rat	snake
turtle	frog	chicken	duck	goose	bee	pig	turkey	fly	llama
camel	bat	gorilla	hedgehog	kangaroo					

TABLE I
SDPO TRAINING HYPERPARAMETERS FOR AESTHETIC SCORE, IMAGEREWARD, HPSV2, AND PICKSCORE.

Hyperparameter	Notation	Aesthetic Score	ImageReward	HPSv2	PickScore
Random seed	–	42	42	42	42
Denoising steps per trajectory	T	50	50	50	50
Classifier-free guidance scale	–	1.0	1.0	1.0	1.0
Maximum gradient norm	–	1.0	1.0	1.0	1.0
Optimizer type	–	AdamW	AdamW	AdamW	AdamW
Optimizer weight decay	–	1×10^{-4}	1×10^{-4}	1×10^{-4}	1×10^{-4}
Optimizer β_1	–	0.9	0.9	0.9	0.9
Optimizer β_2	–	0.999	0.999	0.999	0.999
Optimizer epsilon	–	1×10^{-8}	1×10^{-8}	1×10^{-8}	1×10^{-8}
Learning rate	–	1×10^{-4}	5×10^{-5}	5×10^{-5}	6×10^{-5}
Sampling batch size per GPU	B_1	8	8	8	8
Sampling batches per epoch	–	4	4	4	4
Running statistics buffer size	–	32	32	32	32
Running statistics minimal count	–	16	16	16	16
Training batch size per GPU	B_2	2	1	1	1
Gradient accumulation steps	–	8	32	32	16
Log-ratio scale factor	η	1.0	1.0	1.0	1.0
Clipping range	ϵ	1×10^{-4}	1×10^{-4}	1×10^{-4}	1×10^{-4}
Discount factor	γ	0.99	0.99	0.99	0.99
Decay rate	λ	0.99	0.99	0.99	0.99

B. Additional Setup for Latent Consistency Models

As introduced in Section IV-F of our main manuscript, to finetune the latent consistency model [6], we employ RLCM [7] as our baseline, which integrates both DDPO and REBEL. Based on the official repository of RLCM, we first reproduced the experiments for both DDPO and REBEL. Then, we integrated our SDPO into the RLCM framework, aligning its key hyperparameters with those of REBEL (e.g., *number of inference steps* = 8 and *batches per epoch* = 10), except for SDPO-specific ones (e.g., *discount factor* and *decay rate*), which follow the values in Table I.

C. Additional Setup for Text-to-Multiview Diffusion Models

In Section IV-G of our main manuscript, we present additional results on finetuning a *text-to-multiview* (T2MV) diffusion model, using LCM-SDXL [8] with MV-Adapter [9] as the base model and the HyperScore metric from the MATE-3D benchmark [10] as the reward function. Specifically, we extend our previous implementations within the RLCM framework to finetune this T2MV model, aligning task-specific settings (e.g., *number of views* = 6) with MV-Adapter. For the reward function, we compute the reward for each batch of 6-view images by summing all four dimensions of evaluation scores from the HyperScore model.

APPENDIX B DERIVATIONS

A. The Gradient of the SDPO Objective

As introduced in Section III-D of our main manuscript, the SDPO objective incorporates several components with specific forms of stepwise weighting and clipping. In the following, we derive the gradients for each of these equations. Firstly, the

unclipped SDPO objective is given by:

$$l_\theta(\mathbf{x}_t^a, \mathbf{x}_t^b, \mathbf{c}) = \mathbb{E}_{\mathbf{x}_t^a, \mathbf{x}_t^b, \mathbf{c}} \left[\left(\Delta\rho_t(\theta) \cdot \frac{\lambda^{(T-t-1)}}{\eta} - \Delta\hat{A}_t \right)^2 \right], \quad (1)$$

where $\Delta\rho_t(\theta) := \rho_t^a(\theta) - \rho_t^b(\theta)$ is the difference in log-likelihood ratios, and $\Delta\hat{A}_t := \hat{A}_t^a - \hat{A}_t^b$ is the difference in advantage estimates for trajectories a and b at step t . The gradient of l_θ w.r.t. θ is:

$$\nabla_\theta l_\theta(\mathbf{x}_t^a, \mathbf{x}_t^b, \mathbf{c}) = \mathbb{E}_{\mathbf{x}_t^a, \mathbf{x}_t^b, \mathbf{c}} \left[2 \left(\Delta\rho_t(\theta) \cdot \frac{\lambda^{(T-t-1)}}{\eta} - \Delta\hat{A}_t \right) \cdot \frac{\lambda^{(T-t-1)}}{\eta} \cdot \nabla_\theta \Delta\rho_t(\theta) \right]. \quad (2)$$

To expand $\nabla_\theta \Delta\rho_t(\theta)$, we note that:

$$\nabla_\theta \Delta\rho_t(\theta) = \nabla_\theta \rho_t^a(\theta) - \nabla_\theta \rho_t^b(\theta), \quad (3)$$

where each $\rho_t^j(\theta)$ has a gradient given by:

$$\nabla_\theta \rho_t^j(\theta) = \frac{\nabla_\theta p_\theta(\mathbf{x}_t^j | \mathbf{c})}{p_\theta(\mathbf{x}_t^j | \mathbf{c})}. \quad (4)$$

Substituting it back, we obtain the full gradient for the unclipped objective:

$$\nabla_\theta l_\theta(\mathbf{x}_t^a, \mathbf{x}_t^b, \mathbf{c}) = \mathbb{E}_{\mathbf{x}_t^a, \mathbf{x}_t^b, \mathbf{c}} \left[2 \left(\Delta\rho_t(\theta) \cdot \frac{\lambda^{(T-t-1)}}{\eta} - \Delta\hat{A}_t \right) \cdot \frac{\lambda^{(T-t-1)}}{\eta} \cdot \left(\frac{\nabla_\theta p_\theta(\mathbf{x}_t^a | \mathbf{c})}{p_\theta(\mathbf{x}_t^a | \mathbf{c})} - \frac{\nabla_\theta p_\theta(\mathbf{x}_t^b | \mathbf{c})}{p_\theta(\mathbf{x}_t^b | \mathbf{c})} \right) \right]. \quad (5)$$

To stabilize updates, we constrain the log-likelihood ratios within a trust region by clipping them, yielding the clipped SDPO objective:

$$\tilde{l}_\theta(\mathbf{x}_t^a, \mathbf{x}_t^b, \mathbf{c}) = \mathbb{E}_{\mathbf{x}_t^a, \mathbf{x}_t^b, \mathbf{c}} \left[\left(\Delta\tilde{\rho}_t(\theta) \cdot \frac{\lambda^{(T-t-1)}}{\eta} - \Delta\hat{A}_t \right)^2 \right], \quad (6)$$

where $\Delta\tilde{\rho}_t(\theta) := \tilde{\rho}_t^a(\theta) - \tilde{\rho}_t^b(\theta)$ and $\tilde{\rho}_t^j(\theta) := \text{clip}(\rho_t^j(\theta), -\epsilon, \epsilon)$. The gradient for the clipped objective \tilde{l}_θ w.r.t. θ is:

$$\nabla_\theta \tilde{l}_\theta(\mathbf{x}_t^a, \mathbf{x}_t^b, \mathbf{c}) = \mathbb{E}_{\mathbf{x}_t^a, \mathbf{x}_t^b, \mathbf{c}} \left[2 \left(\Delta\tilde{\rho}_t(\theta) \cdot \frac{\lambda^{(T-t-1)}}{\eta} - \Delta\hat{A}_t \right) \cdot \frac{\lambda^{(T-t-1)}}{\eta} \cdot \nabla_\theta \Delta\tilde{\rho}_t(\theta) \right]. \quad (7)$$

Expanding $\nabla_\theta \Delta\tilde{\rho}_t(\theta)$, we have:

$$\nabla_\theta \Delta\tilde{\rho}_t(\theta) = \nabla_\theta \tilde{\rho}_t^a(\theta) - \nabla_\theta \tilde{\rho}_t^b(\theta), \quad (8)$$

where each $\nabla_\theta \tilde{\rho}_t^j(\theta)$ depends on whether $\rho_t^j(\theta)$ is within the clipping range $[-\epsilon, \epsilon]$. Thus, for each term where $\rho_t^j(\theta)$ is clipped, the gradient will be zero:

$$\nabla_\theta \tilde{\rho}_t^j(\theta) = \begin{cases} \nabla_\theta \rho_t^j(\theta), & \text{if } -\epsilon < \rho_t^j(\theta) < \epsilon, \\ 0, & \text{otherwise.} \end{cases} \quad (9)$$

The final SDPO objective selects the maximum value between the unclipped and clipped objectives, and employs a step-shuffled gradient update strategy. This stepwise policy gradient update is formulated as:

$$\mathcal{L}_t(\theta) \leftarrow \frac{1}{B} \sum_{i=1}^B \max \left(l_\theta(\mathbf{x}_{\tau_i}^{a,i}, \mathbf{x}_{\tau_i}^{b,i}, \mathbf{c}_i), \tilde{l}_\theta(\mathbf{x}_{\tau_i}^{a,i}, \mathbf{x}_{\tau_i}^{b,i}, \mathbf{c}_i) \right), \quad (10)$$

where τ_i represents the shuffled step indices for the i -th batch. For each gradient update, we use the objective value corresponding to the maximum between l_θ and \tilde{l}_θ for each sample in the batch. The gradient of $\mathcal{L}_t(\theta)$ w.r.t. θ is:

$$\nabla_\theta \mathcal{L}_t(\theta) = \frac{1}{B} \sum_{i=1}^B \max \left(\nabla_\theta l_\theta(\mathbf{x}_{\tau_i}^{a,i}, \mathbf{x}_{\tau_i}^{b,i}, \mathbf{c}_i), \nabla_\theta \tilde{l}_\theta(\mathbf{x}_{\tau_i}^{a,i}, \mathbf{x}_{\tau_i}^{b,i}, \mathbf{c}_i) \right). \quad (11)$$

This final gradient facilitates stable and efficient updates across steps by incorporating both the unclipped and clipped objectives in each stepwise update, selecting the one that better preserves stability at each step.

APPENDIX C ADDITIONAL REWARD CURVES

In Section IV-B of our main manuscript, we compared the sample efficiency of different reward finetuning algorithms by showcasing a subset of reward curves for low-step samples. Here we present additional reward curves for 1-step, 2-step, 4-step, and 8-step sampling evaluations in Figs. 1, 2, 3, and 4, respectively. Across all these evaluations, our SDPO consistently demonstrates superior sample efficiency compared to other algorithms.

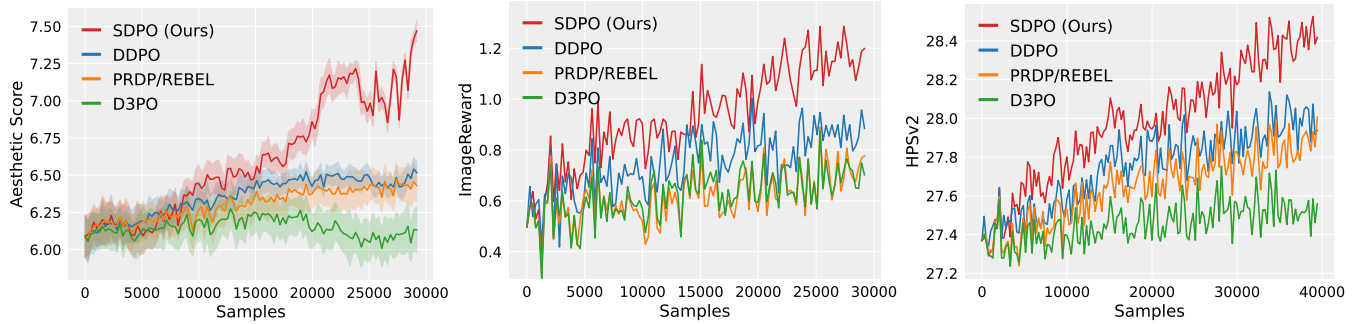


Fig. 1. **Reward curves for 1-step sampling.** Reward scores (left: Aesthetic Score, middle: ImageReward, right: HPSv2) are evaluated for images generated with 1 sampling step. The horizontal axis represents the cumulative number of training samples.

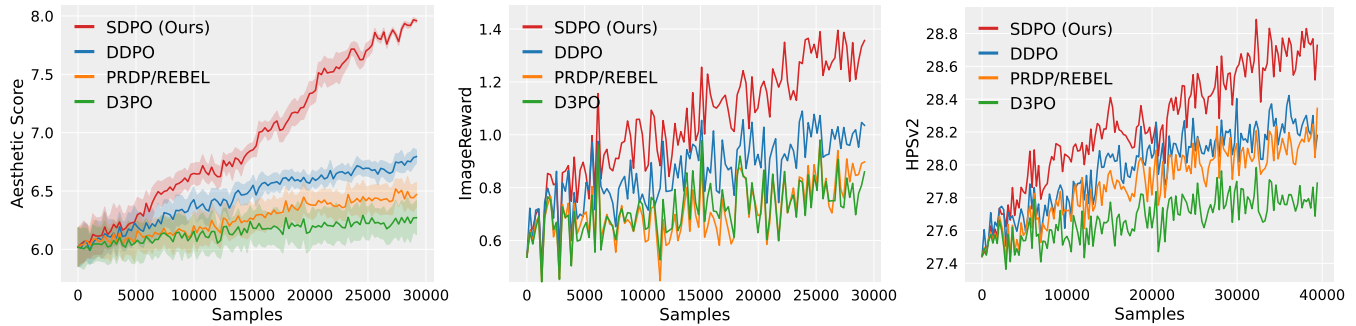


Fig. 2. **Reward curves for 2-step sampling.** Reward scores (left: Aesthetic Score, middle: ImageReward, right: HPSv2) are evaluated for images generated with 2 sampling steps. The horizontal axis represents the cumulative number of training samples.

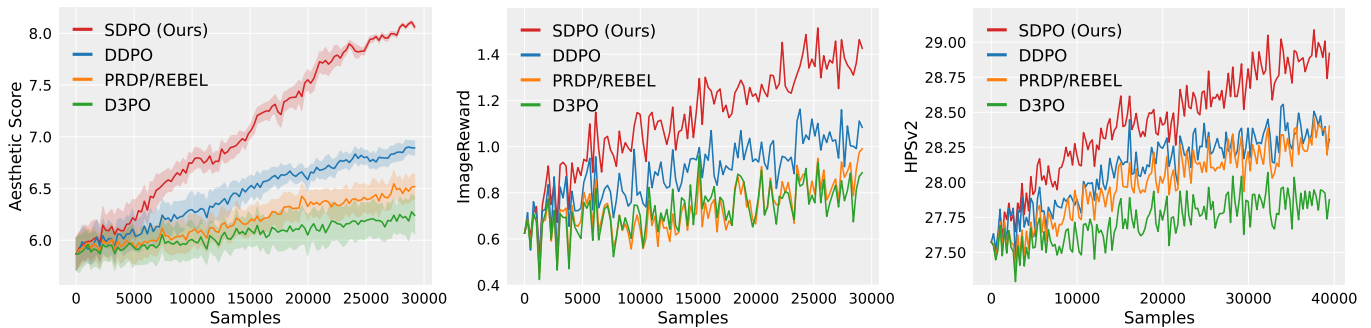


Fig. 3. **Reward curves for 4-step sampling.** Reward scores (left: Aesthetic Score, middle: ImageReward, right: HPSv2) are evaluated for images generated with 4 sampling steps. The horizontal axis represents the cumulative number of training samples.

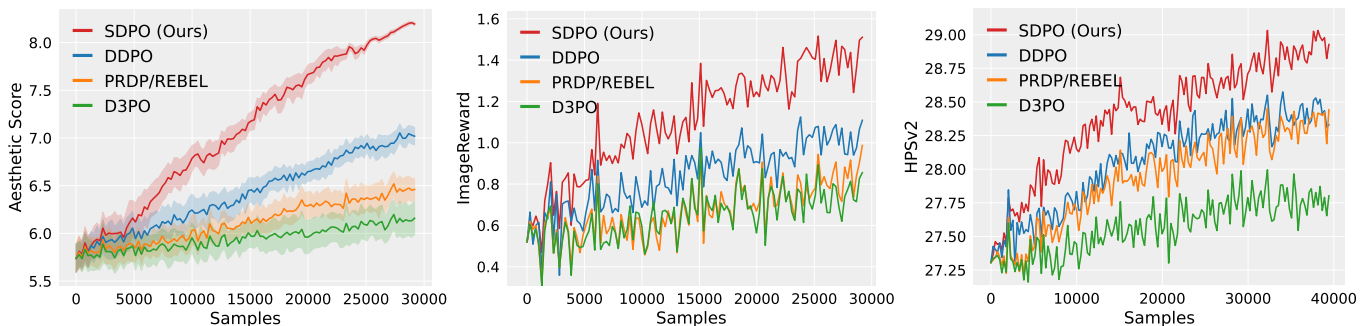


Fig. 4. **Reward curves for 8-step sampling.** Reward scores (left: Aesthetic Score, middle: ImageReward, right: HPSv2) are evaluated for images generated with 8 sampling steps. The horizontal axis represents the cumulative number of training samples.

APPENDIX D
ADDITIONAL QUALITATIVE EXAMPLES

In Fig. 5, 6, 7, 8, 9, and 10, we present additional samples from our SDPO, comparing with DDPO, PRDP/REBEL, D3PO, and pretrained SD-Turbo. While low-step samples from the other methods exhibit lower visual quality and weaker alignment with the target reward structure, our SDPO consistently delivers high-quality, reward-aligned images across all few-step settings.

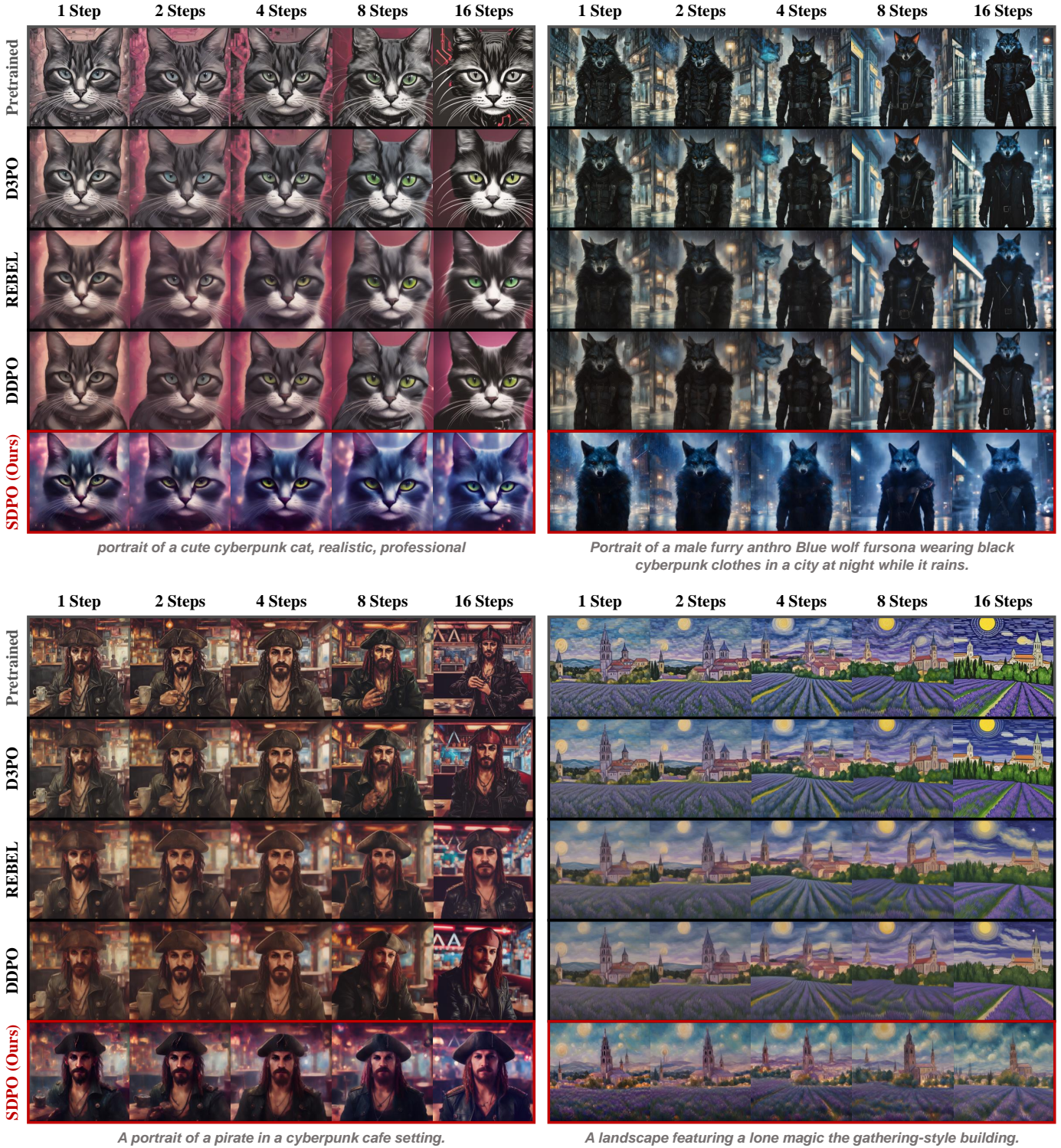


Fig. 5. **Generated images for unseen prompts by:** pretrained SD-Turbo and models finetuned on PickScore, using the same number of training samples. All images are generated with the same random seed. **REBEL** represents the interpolated **PRDP/REBEL** method.

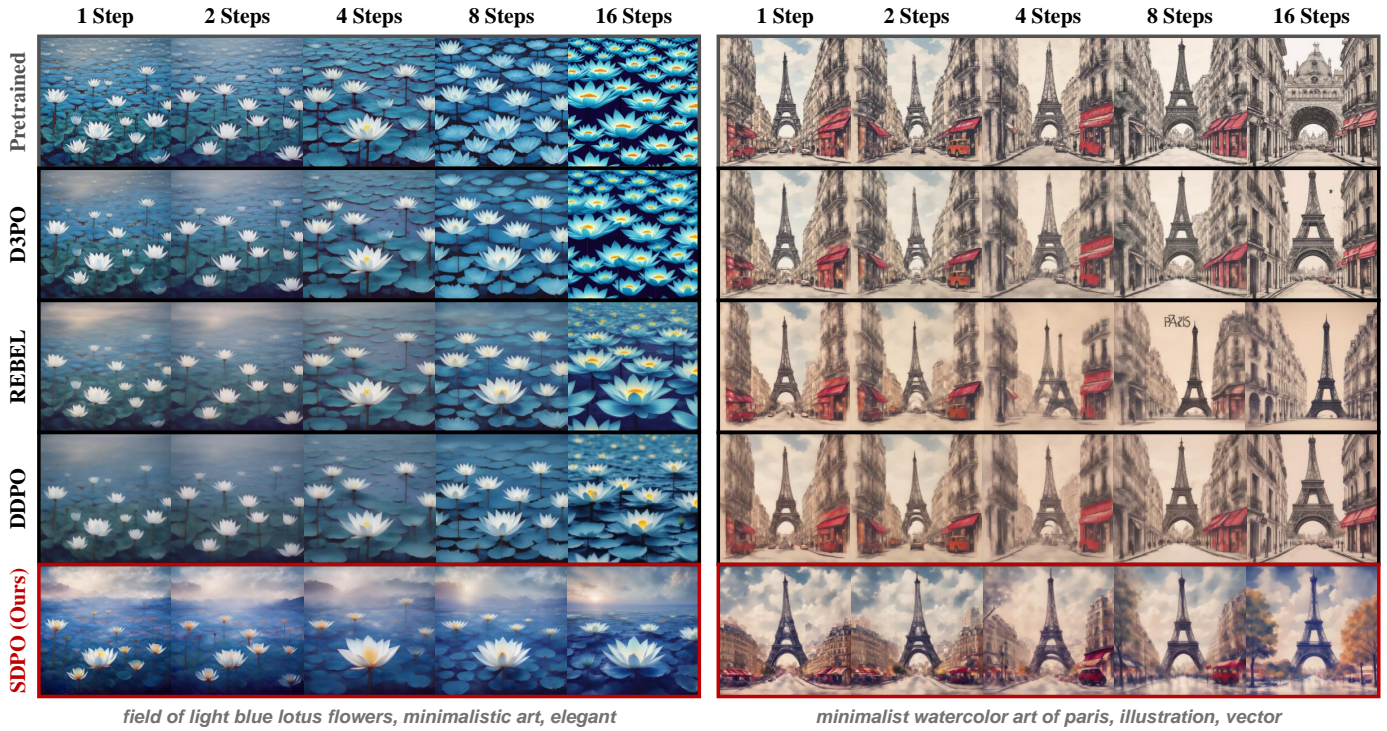


Fig. 6. **Generated images for unseen prompts by:** pretrained SD-Turbo and models finetuned on PickScore, using the same number of training samples. All images are generated with the same random seed. **REBEL** represents the interpolated **PRDP/REBEL** method.

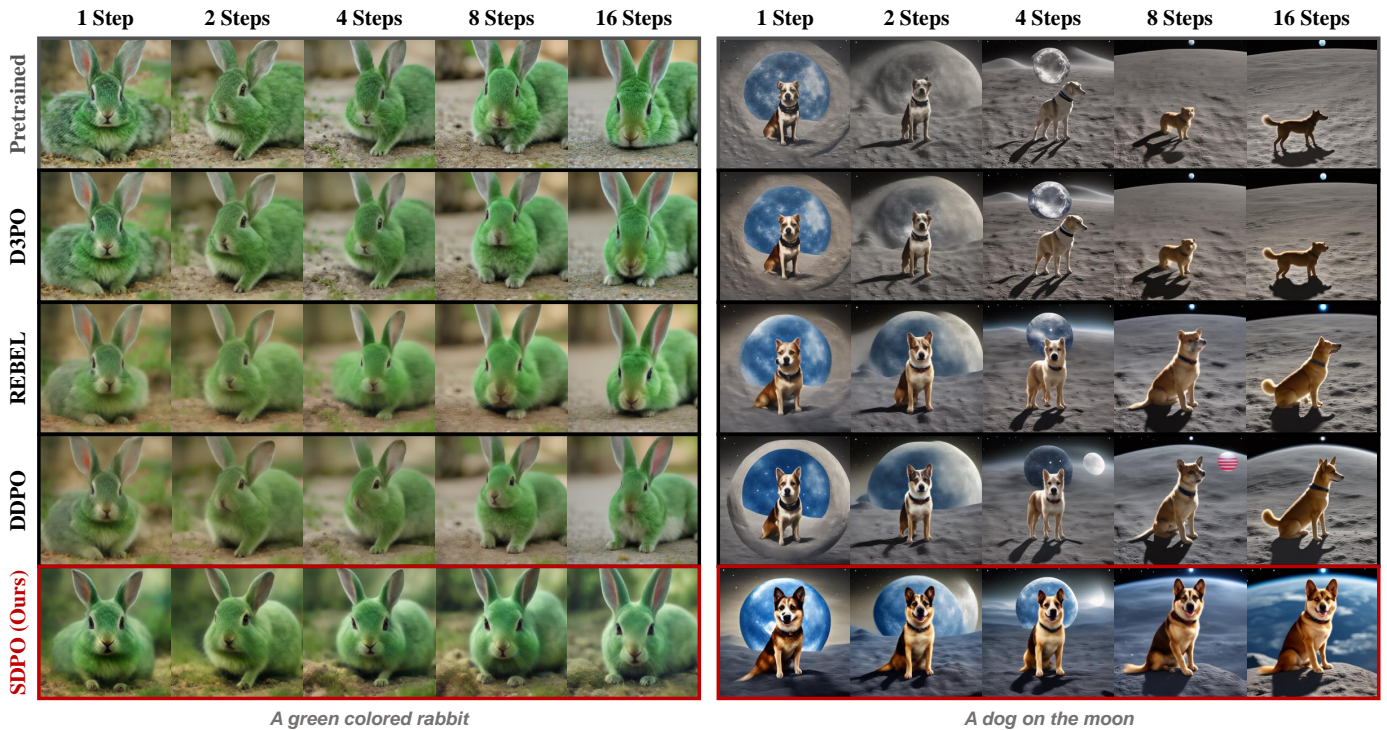


Fig. 7. **Generated images for unseen prompts by:** pretrained SD-Turbo and models finetuned on PickScore (left) and HPSv2 (right), using the same number of training samples. All images are generated with the same random seed. **REBEL** represents the interpolated **PRDP/REBEL** method.

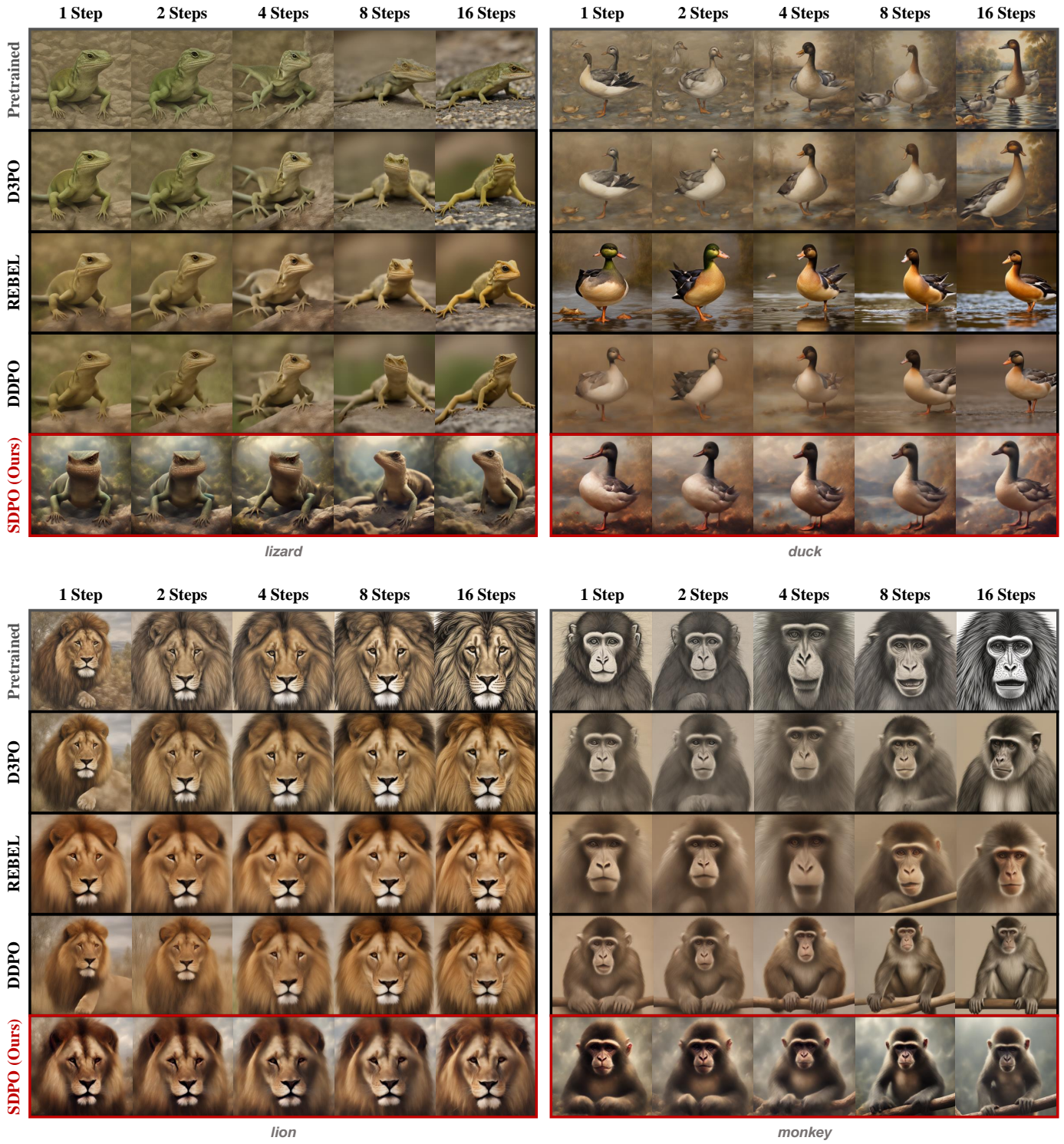


Fig. 8. **Generated images for seen prompts by:** pretrained SD-Turbo and models finetuned on PickScore, using the same number of training samples. All images are generated with the same random seed. **REBEL** represents the interpolated **PRDP/REBEL** method.

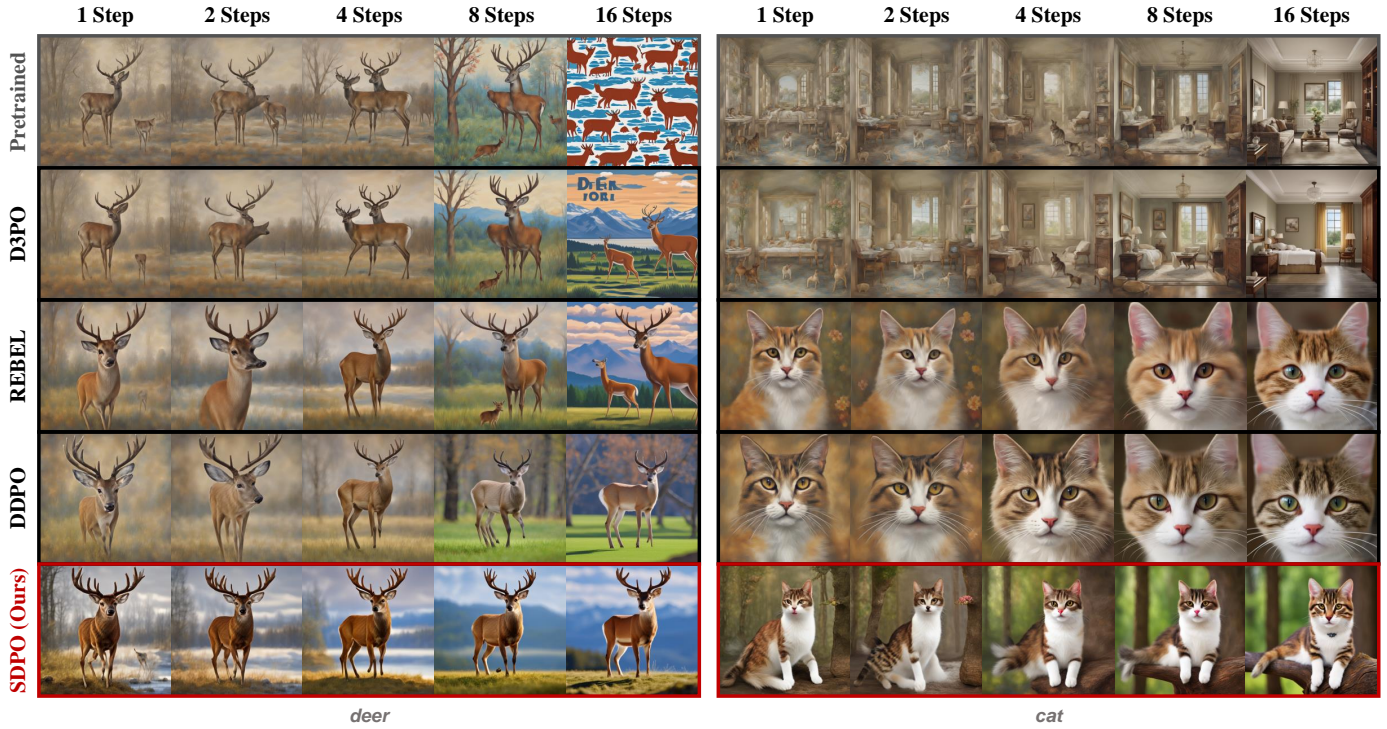


Fig. 9. **Generated images for seen prompts by:** pretrained SD-Turbo and models finetuned on HPSv2, using the same number of training samples. All images are generated with the same random seed. **REBEL** represents the interpolated **PRDP/REBEL** method.

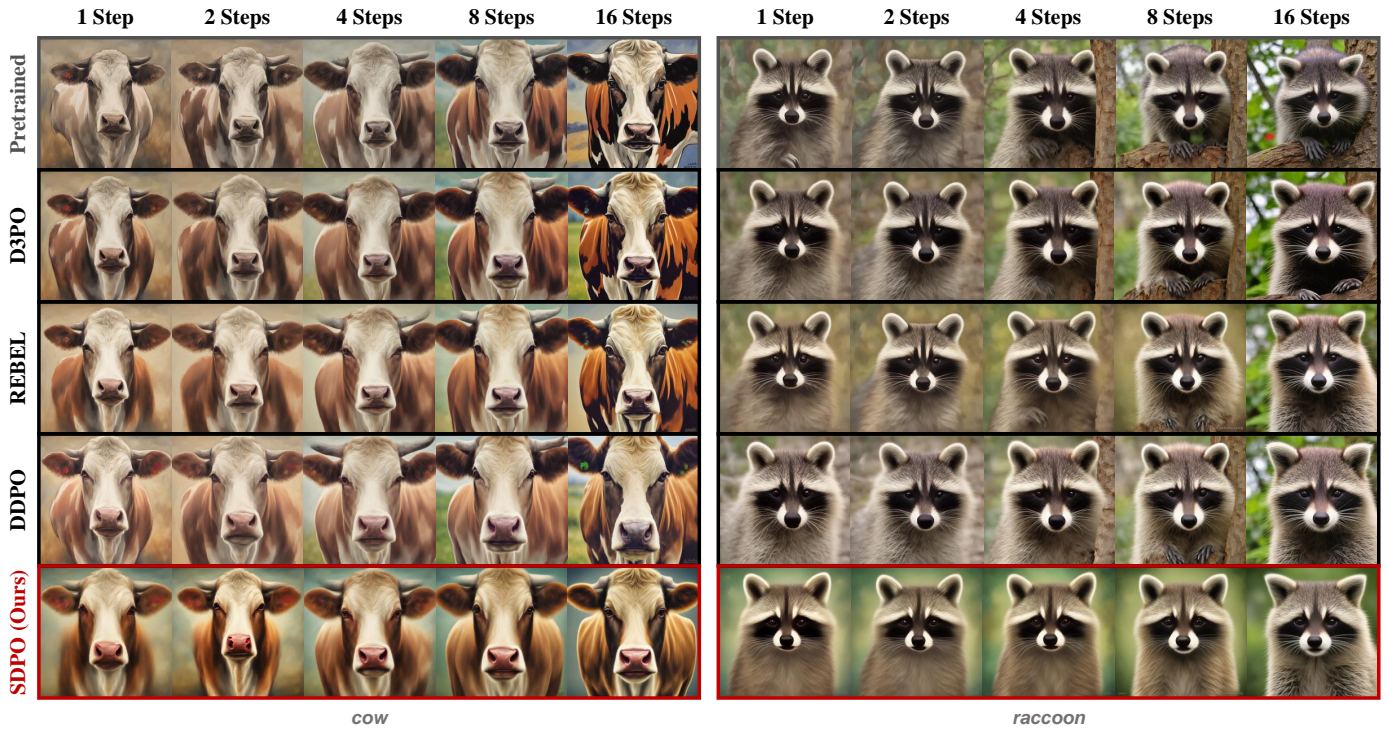


Fig. 10. **Generated images for seen prompts by:** pretrained SD-Turbo and models finetuned on ImageReward, using the same number of training samples. All images are generated with the same random seed. **REBEL** represents the interpolated **PRDP/REBEL** method.

APPENDIX E
VALIDITY OF PREDICTED CLEAN STATES AS SURROGATES FOR ACTUAL t -STEP OUTPUTS

To validate the reliability of predicted clean states as surrogates for actual t -step outputs in capturing the essential characteristics relevant for reward evaluation, we present a comparative analysis of reward scores between these two sample types across a large sample of generated images. Specifically, we evaluate the reward functions used in our experiments (Aesthetic Score, ImageReward, HPSv2, and PickScore) on both predicted clean states and actual outputs for 1-, 2-, 4-, 8-, and 16-step samples generated by the pretrained, non-finetuned SD-Turbo model, and calculated the mean reward differences. The results are summarized in Table II.

TABLE II
REWARD CONSISTENCY BETWEEN PREDICTED CLEAN STATES AND ACTUAL t -STEP OUTPUTS. FOR EACH STEP SETTING (1, 2, 4, 8 STEPS), WE COMPARE MEAN REWARDS ON PREDICTED CLEAN STATES (*Pred*) VERSUS ACTUAL t -STEP OUTPUTS (*Actual*), WITH THEIR ABSOLUTE DIFFERENCE (*Diff*, HIGHLIGHTED). ALL REWARDS ARE REPORTED AS MEAN \pm STANDARD DEVIATION OVER 128 SAMPLES.

Reward Function	1 step			2 steps			4 steps			8 steps		
	<i>Pred</i>	<i>Actual</i>	<i>Diff</i>									
Aesthetic Score	6.08	6.08	0.00	6.05	6.02	0.03	6.01	5.89	0.12	5.92	5.81	0.11
ImageReward	± 0.36	± 0.36	0.00	± 0.39	± 0.40	0.03	± 0.39	± 0.40	0.12	± 0.45	± 0.42	0.11
	0.52	0.52	0.00	0.49	0.57	0.08	0.55	0.51	0.04	0.45	0.53	0.08
HPSv2	± 1.05	± 1.05	0.00	± 1.02	± 1.03	0.08	± 1.00	± 1.06	0.04	± 1.10	± 1.09	0.08
	27.38	27.38	0.00	27.40	27.51	0.11	27.45	27.52	0.07	27.56	27.38	0.18
PickScore	± 0.91	± 0.91	0.00	± 0.99	± 1.10	0.11	± 1.03	± 1.26	0.07	± 1.13	± 1.41	0.18
	21.71	21.71	0.00	21.77	21.82	0.05	21.76	21.79	0.03	21.69	21.58	0.11
	± 0.78	± 0.78	0.00	± 0.80	± 0.87	0.05	± 0.77	± 0.84	0.03	± 0.78	± 0.84	0.11

Notably, the reward scores for predicted clean states and actual t -step outputs in the 1-step setting are identical, which is expected since the predicted clean state is effectively the same as the actual output after one denoising step. For other step settings, the reward differences between the predicted clean states and the actual outputs are consistently smaller than the standard deviations of reward scores, indicating that the differences are relatively minor compared to the overall variability in reward scores and thereby exhibiting substantial reward consistency between the two sample types. This supports our claim that the predicted clean states can serve as reliable surrogates that capture the essential characteristics relevant for reward evaluation, thereby justifying their use in our dense reward prediction framework.

However, it is important to note that, even if the reward differences were to exceed the standard deviations, the predicted clean states could still be valid surrogates as long as they preserve the relative ranking of rewards among different samples. This is ensured not only by the Lipschitz continuity property of the reward functions, but also by our effective design of the dense reward learning objective, which guides policy optimization based on the relative differences in dense rewards rather than their absolute values.

APPENDIX F
EMPIRICAL ANALYSIS OF LIPSCHITZ CONTINUITY ACROSS REWARD FUNCTIONS

To validate the Lipschitz continuity assumption underlying our dense reward prediction approach, we present an empirical analysis of the Lipschitz constants for different reward functions used in our experiments, which are computed as the ratios of reward differences to latent distances across a large sample of full denoising trajectories generated by the pretrained, non-finetuned SD-Turbo model. Specifically, within each denoising trajectory, we compute the predicted clean states for all step pairs (i, j) where $i < j$ and calculate the following statistics for each pair of clean states: (1) *Latent distance*: $\|\phi(\hat{\mathbf{x}}_0^i) - \phi(\hat{\mathbf{x}}_0^j)\|$, where ϕ denotes the latent representations directly obtained from the denoising process; (2) *Reward change*: $|R(\hat{\mathbf{x}}_0^i, \mathbf{c}) - R(\hat{\mathbf{x}}_0^j, \mathbf{c})|$, computed on the decoded clean images of predicted clean states and standardized to the range $[0, 1]$ for fair comparison across reward functions with different scales; and (3) *Lipschitz ratio*: the ratio of reward change to latent distance $|\Delta R|/\|\Delta\phi\|$. We then aggregate these ratios across all step pairs and trajectories to obtain the maximum, mean, median, 95th percentile, and 99th percentile values for each reward function, where the maximum value serves as an empirical estimate of the Lipschitz constant. The results are summarized in Table III.

As shown in Table III, the empirical Lipschitz constants remain consistently small across all reward functions, with maximum values ranging from 0.001809 to 0.002536. This narrow range demonstrates that Lipschitz continuity is a universal characteristic of reward functions in the latent space of diffusion models, rather than an artifact of particular reward designs. More importantly, the distribution statistics reveal highly concentrated Lipschitz ratios. The mean values are 8-14 times smaller than the maximum across all reward functions, while the median values are even lower (9-22 times smaller). Even the 99th percentiles consistently remain below 50% of their respective maximum values—for instance, 39% for Aesthetic Score (0.000981 vs. 0.002536) and 38% for ImageReward (0.000940 vs. 0.002461). This concentration demonstrates that large Lipschitz ratios are exceedingly rare, with typical reward transitions being far smoother than worst-case bounds.

TABLE III

EMPIRICAL LIPSCHITZ CONSTANTS AND DISTRIBUTION STATISTICS FOR DIFFERENT REWARD FUNCTIONS. THE MAXIMUM LIPSCHITZ RATIO (HIGHLIGHTED) SERVES AS THE EMPIRICAL LIPSCHITZ CONSTANT, WHILE THE OTHER COLUMNS SHOW THE MEAN, MEDIAN, AND 95TH/99TH PERCENTILE OF ALL RATIOS, ALL COMPUTED ON REWARDS NORMALIZED TO $[0, 1]$ ACROSS 156800 STEP PAIRS FROM FULL DENOISING TRAJECTORIES.

Reward Function	Max (Lipschitz Constant)	Mean Ratio	Median Ratio	95th Percentile	99th Percentile
Aesthetic Score	0.002536	0.000265	0.000206	0.000711	0.000981
ImageReward	0.002461	0.000174	0.000111	0.000588	0.000940
HPSv2	0.002483	0.000197	0.000155	0.000519	0.000725
PickScore	0.001809	0.000236	0.000191	0.000609	0.000870

APPENDIX G

COMPARISON OF PEAK GPU MEMORY USAGE DURING RL FINETUNING

In this appendix, we compare the peak GPU memory usage during RL finetuning between our SDPO and other methods, including D3PO, DDPO, REBEL, as well as several SDPO variants from our ablation study. The results, summarized in Table IV, indicate that all the evaluated methods have comparable GPU memory usage during training. This is expected, as they share the same underlying diffusion model architecture and batch size. The primary differences lie in reward computation strategies, which can affect computation time but have minimal impact on memory usage. This supports our GPU runtime comparison in the main manuscript as an effective measure of training efficiency differences among the methods.

TABLE IV

COMPARISON OF PEAK GPU MEMORY USAGE DURING RL FINETUNING ACROSS DIFFERENT METHODS.

Method	Peak GPU Memory (GiB)
D3PO	23.38
DDPO	22.73
REBEL	23.78
SDPO variant (1 query & copy)	23.33
SDPO variant (2 queries & interpolation)	23.46
SDPO variant (2 queries & similarity)	23.45
SDPO variant (3 queries & similarity & fixed anchor)	23.33
SDPO variant (3 queries & similarity & random anchor)	23.33
SDPO variant (Full-step queries)	23.47
SDPO (Ours)	23.32

APPENDIX H

EFFECTIVENESS OF STEP-SHUFFLED UPDATES IN PREVENTING STEP OVERFITTING

In this appendix, we present an additional quantitative analysis of the effectiveness of step-shuffled updates in preventing overfitting to step order. In the main manuscript, we compare two gradient update strategies for SDPO: (1) *Step-shuffled updates*, which randomize the order of denoising steps during training, and (2) *Stepwise updates without shuffling*, which follow a fixed step order. As shown in Fig. 6 (right) of the main manuscript, the step-shuffled variant achieves higher reward scores and faster convergence, suggesting that step shuffling helps the model generalize across different step configurations rather than overfit to a specific sequence. To further substantiate this claim with quantitative evidence, we analyze the variance of dense rewards for both variants across multiple denoising trajectories.

Specifically, for each step setting (2, 4, 8, and 16 steps), we generate 128 complete denoising trajectories using each variant and compute dense rewards at every intermediate step along each trajectory. We then calculate three complementary variance metrics: (1) *Sample-wise variance*: the variance of rewards across sampling steps within each trajectory, averaged over all 128 trajectories—this metric directly captures reward uniformity across different steps for individual samples; (2) *Step-wise variance*: the variance of rewards across all 128 trajectories at each sampling step, averaged over all steps—this reflects consistency across different samples at the same step; and (3) *Overall variance*: the total variance across all trajectories and steps. The results are summarized in Table V.

As shown in Table V, the step-shuffled variant consistently achieves substantially lower variance across all metrics, step settings, and reward functions. Among all metrics, the sample-wise variance is particularly informative, as it directly measures the uniformity of rewards across different sampling steps within each individual sample—a key indicator of whether the model has learned to generalize across step orders rather than overfit to a fixed sequence. Notably, for the Aesthetic Score reward, the sample-wise variance is reduced by approximately 79–84% (from 0.37–0.43 to 0.07–0.08) when using step shuffling. Even more dramatic reductions are observed for ImageReward, where the sample-wise variance drops by over 98% (from 0.43–0.53 to 0.001–0.014). For HPSv2 and PickScore, the reductions are similarly substantial, with sample-wise variance decreasing by 80–85% (from $5.8e-5$ – $7.2e-5$ to $9e-6$ – $1.2e-5$) and 87–92% (from $4.4e-5$ – $4.9e-5$ to $4e-6$ – $6e-6$), respectively. These consistent

and substantial reductions in variance provide strong quantitative evidence that step-shuffled updates effectively prevent the model from overfitting to a fixed step order, leading to more uniform reward distributions and improved generalization across different step configurations.

TABLE V

REWARD VARIANCE ANALYSIS FOR SDPO VARIANTS WITH AND WITHOUT STEP SHUFFLING. LOWER VARIANCE REFLECTS MORE CONSISTENT REWARDS ACROSS STEPS OR SAMPLES, SUGGESTING REDUCED OVERFITTING TO SPECIFIC STEP SETTINGS. SAMP.: SAMPLE-WISE VARIANCE; STEP.: STEP-WISE VARIANCE; OVER.: OVERALL VARIANCE.

Steps	Variant	Aesthetic Score			ImageReward			HPSv2			PickScore		
		Samp.	Step.	Over.	Samp.	Step.	Over.	Samp.	Step.	Over.	Samp.	Step.	Over.
2	unshuffled	0.377	0.071	0.422	0.528	1.207	1.517	5.8e-5	9.2e-5	1.4e-4	4.4e-5	6.8e-5	1.0e-4
	shuffled	0.078	0.034	0.098	1.1e-3	5.5e-3	5.7e-3	9.0e-6	9.0e-5	9.5e-5	4.0e-6	5.2e-5	5.5e-5
4	unshuffled	0.372	0.074	0.411	0.516	1.485	1.753	6.1e-5	9.8e-5	1.4e-4	4.7e-5	8.7e-5	1.2e-4
	shuffled	0.069	0.025	0.078	1.4e-2	2.3e-2	2.4e-2	1.2e-5	9.8e-5	1.0e-4	6.0e-6	5.9e-5	6.1e-5
8	unshuffled	0.378	0.068	0.414	0.437	1.542	1.727	6.2e-5	1.1e-4	1.5e-4	4.8e-5	9.8e-5	1.3e-4
	shuffled	0.075	0.022	0.081	7.6e-3	1.6e-2	1.8e-2	1.1e-5	1.0e-4	1.1e-4	4.0e-6	6.0e-5	6.2e-5
16	unshuffled	0.434	0.067	0.470	0.450	1.529	1.715	7.2e-5	1.1e-4	1.6e-4	4.9e-5	1.0e-4	1.3e-4
	shuffled	0.071	0.018	0.076	8.0e-3	1.8e-2	2.0e-2	1.1e-5	1.1e-4	1.1e-4	4.0e-6	6.1e-5	6.2e-5

APPENDIX I

RATIONALE AND ADVANTAGES OF REWARD DIFFERENCE LEARNING IN SDPO

In our SDPO framework, we employ reward difference learning [3], [4] to reformulate policy optimization as regressing reward differences onto log-likelihood differences across trajectory pairs. This approach yields surrogate updates that focus on *relative improvements* rather than absolute reward values, thereby mitigating the high variance associated with conventional policy-gradient methods that rely on absolute reward scales. Although our dense reward feedback and stepwise policy update mechanisms could also enhance standard policy gradient methods such as DDPO [2], their gradient estimators remain inherently susceptible to inter-step variances along trajectories, limiting their ability to fully exploit the advantages of dense rewards. In contrast, reward difference learning mitigates this issue by comparing trajectory pairs, thereby facilitating more stable and efficient policy optimization.

To substantiate these claims, we implement a DDPO variant incorporating our dense reward feedback and stepwise policy update mechanisms (denoted as “DDPO w/ DR”), while excluding refinements specific to the reward difference learning objective, as they are not directly applicable to standard policy gradient methods. As shown in Figure 11, this variant improves upon standard DDPO but still underperforms SDPO across 2-step, 4-step, and 8-step sampling evaluations. These results demonstrate that while dense rewards offer clear benefits, the reward difference learning paradigm also provides significant improvements in sample efficiency. Together, they complement each other synergistically, forming a mutual fit that elevates the overall performance of our framework, making reward difference learning a necessary component for optimal results.

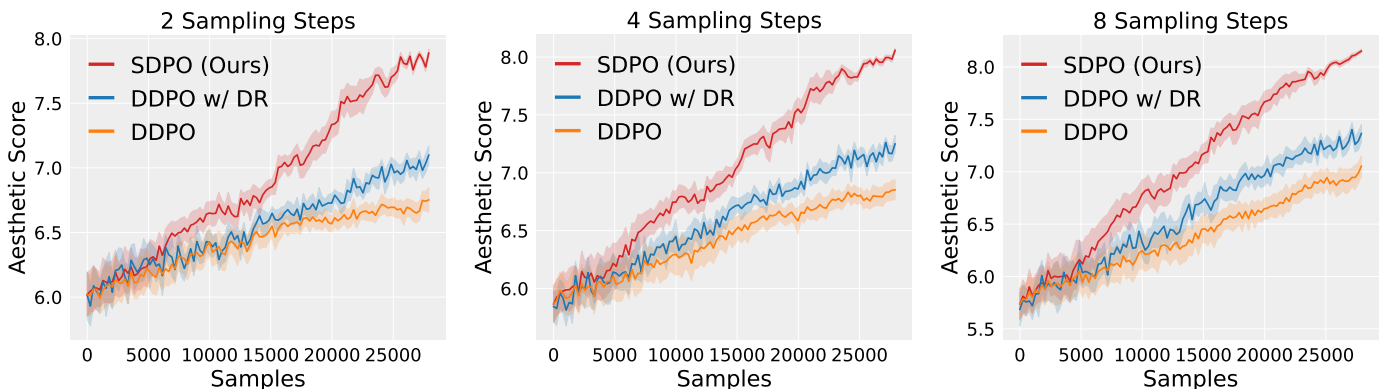


Fig. 11. Comparison of reward curves among SDPO, DDPO, and a **DDPO variant incorporating dense reward feedback and stepwise policy updates** (denoted as “DDPO w/ DR”) across 2-step, 4-step, and 8-step sampling evaluations.

APPENDIX J

ANALYSIS OF COMPLEMENTARY MECHANISMS FOR ENHANCING DENSE REWARD UTILIZATION IN SDPO

In Section III-D, we introduced additional mechanisms such as per-step-prompt normalization and temporal importance weighting to further exploit the advantages of dense rewards within our stepwise optimization framework. It is important to clarify that these designs are not introduced to compensate for any unreliability or deficiencies in the dense rewards, but rather serve as complementary mechanisms that enhance the effectiveness of our core dense reward strategy. Specifically, per-step-prompt normalization leverages the dense reward structure to standardize rewards at each step, thereby reducing variance and stabilizing learning dynamics. Similarly, temporal importance weighting prioritizes updates at earlier trajectory steps, which exert a more pronounced influence on the foundational structure of generated outputs and contribute more significantly to few-step denoising performance, thus enhancing overall optimization efficiency. Both mechanisms are designed to better harness the informative signals provided by our dense rewards for more effective policy updates, rather than serving as necessary corrections for any inherent issues with the dense rewards themselves.

To further validate that our core dense reward strategy is effective independently of these complementary mechanisms, we conduct additional ablation experiments comparing an SDPO variant that employs only our core strategies for dense rewards and stepwise updates (denoted as “SDPO (Core-only)” in Fig. 12)—without per-step-prompt normalization or temporal importance weighting—against baseline methods. As shown in Fig. 12, even this stripped-down variant consistently outperforms all baseline methods across 2-step, 4-step, and 8-step sampling evaluations. This result provides strong evidence that our dense reward predictions are inherently reliable and effective for policy optimization, independent of the additional mechanisms. While the complementary mechanisms further enhance performance, they are not strictly necessary for the core dense reward strategy to yield significant improvements over baselines that rely solely on sparse rewards at the final step.

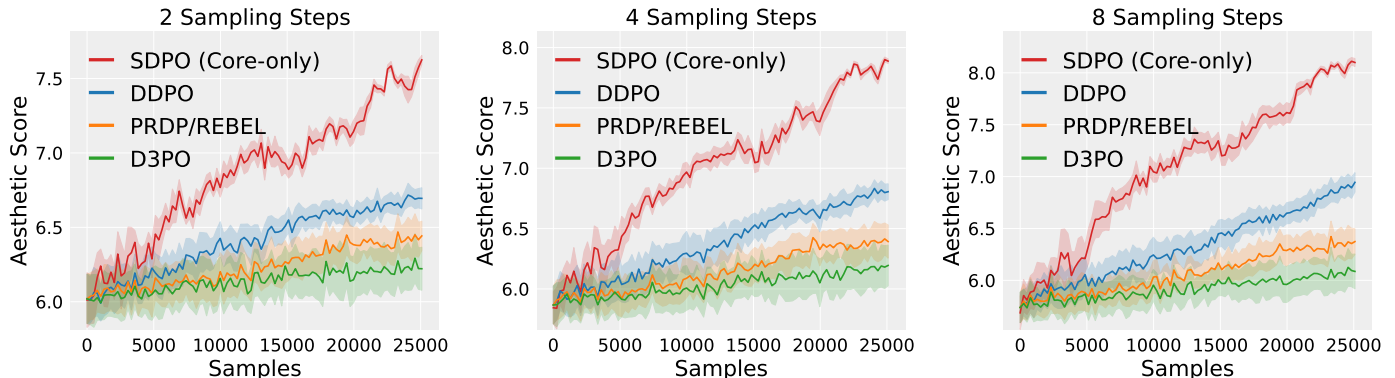


Fig. 12. Additional ablation results comparing the **SDPO variant that uses only our core strategies for dense rewards and stepwise updates** (denoted as “SDPO (Core-only)”) against baseline methods across 2-step, 4-step, and 8-step sampling evaluations.

APPENDIX K

ADDITIONAL ANALYSIS ON THE EFFECTIVENESS OF DENSE REWARDS IN SDPO

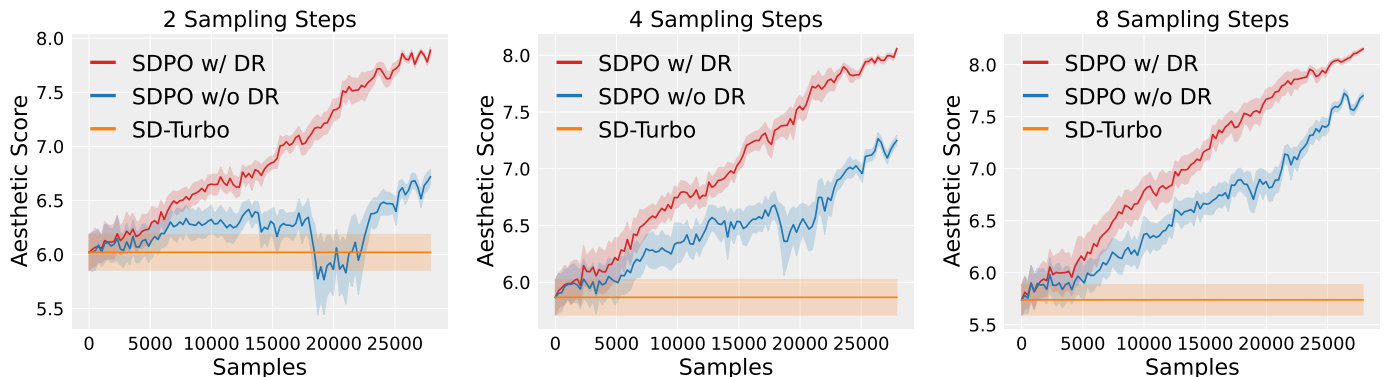


Fig. 13. Comparison of reward curves among **SD-Turbo**, **SDPO without dense rewards**, and **SDPO with dense rewards** (denoted as “SDPO w/o DR” and “SDPO w/ DR”, respectively) across 2-step, 4-step, and 8-step sampling evaluations.

To further demonstrate the contribution and effectiveness of our dense reward design, here we present a direct comparison between SD-Turbo and SDPO without dense rewards. Fig. 13 illustrates the reward curves for 2-step, 4-step, and 8-step sampling

evaluations during training. As shown, despite that the rest of the SDPO framework is designed to take the full advantage of dense rewards, SDPO without dense rewards already achieves notable improvements over SD-Turbo across all sampling step settings, demonstrating the effectiveness of our SDPO framework even without the dense reward design. Moreover, incorporating dense rewards in SDPO leads to significant additional improvements, highlighting the substantial contribution of our dense reward design in achieving superior alignment with desired reward signals in few-step diffusion models.

APPENDIX L

ADDITIONAL ANALYSIS ON REWARD OVEROPTIMIZATION VIA CROSS-REWARD GENERALIZATION EVALUATION

To assess reward overoptimization, we conduct a cross-reward generalization evaluation following the protocol established in prior work [11], [12]. This evaluation assesses whether optimizing for one reward function leads to degradation in other independent reward metrics, which is a key indicator of overoptimization. Specifically, we evaluate the cross-reward generalization performance between ImageReward and Aesthetic Score for SDPO and all baseline methods. We deliberately select these two reward functions because they represent potentially conflicting objectives: Aesthetic Score focuses solely on visual aesthetics without text input, while ImageReward incorporates text prompts to evaluate semantic alignment between generated images and input text. This makes them an ideal pair for assessing reward overoptimization, as optimizing one should not necessarily improve the other if the model is overoptimizing in a narrow sense.

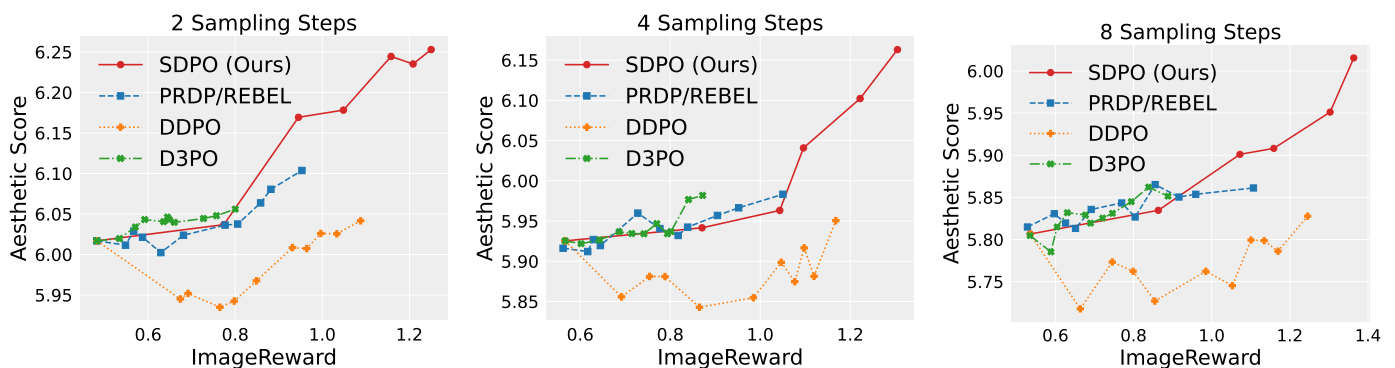


Fig. 14. **Cross-reward generalization evaluation results** when training on ImageReward and evaluating on Aesthetic Score under 2-step, 4-step, and 8-step sampling. SDPO demonstrates strong cross-reward generalization across all sampling step settings while achieving superior target reward optimization, indicating minimal overoptimization.

As shown in Fig. 14, we present the cross-reward generalization results when training on ImageReward and evaluating on Aesthetic Score across different sampling steps. The three subfigures show the results for 2-step (left), 4-step (middle), and 8-step (right) sampling, respectively. Across all sampling step settings, SDPO not only achieves superior target rewards but also demonstrates consistent improvements on out-of-distribution rewards, indicating strong cross-reward generalization and minimal overoptimization. In contrast, baseline methods show only marginal reward improvements within a similar amount of training time, particularly D3PO which exhibits very slow convergence in the few-step regime. Thus, we present the maximum reward values that baseline methods can attain within a reasonable training budget. These results clearly demonstrate that SDPO exhibits low reward overoptimization while achieving superior sample efficiency compared to all baseline methods.

REFERENCES

- [1] A. Sauer, D. Lorenz, A. Blattmann, and R. Rombach, “Adversarial diffusion distillation,” in *European Conference on Computer Vision*, 2024, pp. 87–103.
- [2] K. Black, M. Janner, Y. Du, I. Kostrikov, and S. Levine, “Training diffusion models with reinforcement learning,” in *International Conference on Learning Representations*, 2024.
- [3] F. Deng, Q. Wang, W. Wei, T. Hou, and M. Grundmann, “PRDP: Proximal reward difference prediction for large-scale reward finetuning of diffusion models,” in *Proceedings of the IEEE/CVF Conference on Computer Vision and Pattern Recognition*, 2024, pp. 7423–7433.
- [4] Z. Gao, J. D. Chang, W. Zhan, O. Oertell, G. Swamy, K. Brantley, T. Joachims, J. A. Bagnell, J. D. Lee, and W. Sun, “Rebel: Reinforcement learning via regressing relative rewards,” *Advances in Neural Information Processing Systems*, vol. 37, pp. 52 354–52 400, 2024.
- [5] K. Yang, J. Tao, J. Lyu, C. Ge, J. Chen, W. Shen, X. Zhu, and X. Li, “Using human feedback to fine-tune diffusion models without any reward model,” in *Proceedings of the IEEE/CVF Conference on Computer Vision and Pattern Recognition*, 2024, pp. 8941–8951.
- [6] S. Luo, Y. Tan, L. Huang, J. Li, and H. Zhao, “Latent Consistency Models: Synthesizing high-resolution images with few-step inference,” *arXiv preprint arXiv:2310.04378*, 2023.
- [7] O. Oertell, J. D. Chang, Y. Zhang, K. Brantley, and W. Sun, “RL for consistency models: Reward guided text-to-image generation with fast inference,” *Reinforcement Learning Journal*, vol. 4, pp. 1656–1673, 2024.
- [8] LCM Team, “latent-consistency/lcm-sd-xl,” HuggingFace, 2023.
- [9] Z. Huang, Y.-C. Guo, H. Wang, R. Yi, L. Ma, Y.-P. Cao, and L. Sheng, “MV-Adapter: Multi-view consistent image generation made easy,” in *Proceedings of the IEEE/CVF International Conference on Computer Vision*, 2025, pp. 16 377–16 387.
- [10] Y. Zhang, B. Cui, Q. Yang, Z. Li, and Y. Xu, “Benchmarking and learning multi-dimensional quality evaluator for text-to-3D generation,” in *Proceedings of the IEEE/CVF International Conference on Computer Vision*, 2025, pp. 18 563–18 574.
- [11] Z. Zhang, S. Zhang, Y. Zhan, Y. Luo, Y. Wen, and D. Tao, “Confronting reward overoptimization for diffusion models: A perspective of inductive and primacy biases,” in *International Conference on Machine Learning*, 2024, pp. 60 396–60 413.
- [12] Z. Zhang, S. Zhang, L. Shen, Y. Zhan, Y. Luo, H. Hu, B. Du, Y. Wen, and D. Tao, “Aligning text-to-image diffusion models with constrained reinforcement learning,” *IEEE Transactions on Pattern Analysis and Machine Intelligence*, vol. 47, no. 11, pp. 9550–9562, 2025.